BBA - Bioenergetics 1858 (2017) 854–864

Contents lists available at ScienceDirect

BBA - Bioenergetics

journal homepage: www.elsevier.com/locate/bbabio

A four state parametric model for the kinetics of the non-photochemical quenching in Photosystem II

Joris J. Snellenburg[a], Matthew P. Johnson[b], Alexander V. Ruban[c], Rienk van Grondelle[a], Ivo H.M. van Stokkum[a,*]

[a] Institute for Lasers, Life and Biophotonics, Faculty of Sciences, VU University Amsterdam, De Boelelaan 1081, 1081 HV Amsterdam, The Netherlands.
[b] Department of Molecular Biology and Biotechnology, University of Sheffield, UK
[c] School of Biological and Chemical Sciences, Queen Mary University of London, UK

ARTICLE INFO

Keywords:
Fluorescence quenching analysis
Non-photochemical quenching
Parameter estimation
Time-resolved fluorescence spectroscopy

ABSTRACT

The phenomenon of non-photochemical quenching (NPQ) was studied in spinach chloroplasts using pulse amplitude modulated (PAM) fluorometry. We present a new analysis method which describes the observed fluorescence quantum yield as the sum of the product of four different states of PSII and their corresponding quantum yields. These four distinct states are PSII in the quenched or unquenched state, and with its reaction center either open or closed depending upon the reduction of the Q_A site. With this method we can describe the dynamics of the NPQ induction and recovery as well as quantify the percentage of photoinactivated RC throughout the measurement. We show that after one cycle of quenching followed by a period of recovery, approximately 8–9% of the RC are photoinactivated, after two cycles of illumination this number becomes 15-17%. The recovery from the quenching appeared with rates of $(50\ s)^{-1}$ and $(1\ h)^{-1}$. The new analysis method presented here is flexible, allowing it to be applied to any type of PAM fluorometry protocol. The method allows to quantitatively compare qualitatively different PAM curves on the basis of statistically relevant fitting parameters and to quantify quenching dynamics and photoinactivation. Moreover, the results presented here demonstrate that the analysis of a single PAM fluorometry quenching experiment can already provide information on the relative quantum yield of the four different states of PSII for the intact chloroplasts - something no other form of spectroscopy could provide in a single measurement.

1. Introduction

Non-photochemical quenching (NPQ) has long been in the focus of photosynthesis research [1]. Recently, the fundamental knowledge on the kinetic aspects of NPQ has been utilized in the creation of highly productive crops [2]. Therefore it is essential to create a model describing these kinetics in order to obtain key physiological parameters of Photosystem II (PSII) activity.

Pulse amplitude modulation (PAM) fluorometry is a technique which can be used to measure the fluorescence quantum yield even in the presence of actinic light [3,4], and as such can be performed in a wide range of physiological conditions. The required equipment is relatively inexpensive and can even be carried into the field [5].

The fluorescence detected by a PAM fluorometer originates from all pigment-protein complexes that absorb light at the excitation wavelength used and emit fluorescence overlapping with its detector window (typically $\lambda > 700$ nm). Modulation is used to ensure that the recorded signal is due to the (constant) modulated measuring light only. Any increase or decrease in the recorded signal can directly be related to changes in the fluorescence quantum yield of the different pigment protein complexes.

Theoretical models of the light dependent reactions in the thylakoid membrane can predict a PAM signal, which can be used to verify such models. The (fast) kinetics of chlorophyll fluorescence induction is described in e.g. [6–8] reviewed in [9,10] and more recently [11]. The slower processes such as NPQ and state transitions, are modelled in [12–16].

Here we start not from theory, but from the experimental data, and analyze the PAM signals of various intact chloroplasts obtained using a typical light protocol used for quenching analysis experiments [17], and quantify the dynamically changing concentrations of the different emissive species. The artificial electron acceptor methylviologen was

Abbreviations: Chl, chlorophyll; GA, glutaraldehyde; LHC, light harvesting complex; LR, light regime; NPQ, non-photochemical quenching; PAM, pulse amplitude modulation; PSI, Photosystem I; PSII, Photosystem II; RC, reaction center; SP, saturating pulse; V, devoid of zeaxanthin; Z, (enriched in) zeaxanthin

* Corresponding author.
E-mail address: ivo@few.vu.nl (I.H.M. van Stokkum).

http://dx.doi.org/10.1016/j.bbabio.2017.08.004
Received 27 January 2017; Received in revised form 12 July 2017; Accepted 5 August 2017
Available online 08 August 2017
0005-2728/

used in this study to promptly obtain a stable level of the proton gradient, the trigger for NPQ, upon illumination. This was a simplification of an experimental scheme in order to avoid further complexity of the modelling process and therefore minimize the number of variables. In our approach we explicitly assume a discrete number of states for the contribution of PSII. It can be quenched or unquenched and switches between these extremes due to changes in the actinic light. At the same time it can be open or closed dependent on the reduction state of Q_A of the PSII RC, resulting in a total of four discrete states for PSII. Apart from PSII which dominates the signal there are other emissive species that contribute to the fluorescence quantum yield, e.g. PSI [18,19], disconnected antenna complexes such as light harvesting complex I and II (LHCI and LHCII [20] respectively). The relative concentrations and the quantum yields of different emissive species depend on the organism, growing conditions, mutations, chemical treatments, etc. We employ a parametric model which takes the light protocol and the high quality measurements as input and aims to describe the data up to the noise level, in order to extract all the information available. The method is flexible enough to analyze multiple measurements (e.g. different preparations, different mutations) following the same protocol simultaneously, while linking parameters between datasets that are expected to be conserved, i.e. global analysis of PAM fluorometry data. In this way it is possible to more reliably quantify differences in photosynthetic efficiency or stoichiometry of the photosynthetic complexes between experiments. To illustrate this point, measurements on intact chloroplasts, prepared in a way that they were either devoid of zeaxanthin (V) or enriched in zeaxanthin (Z), are used as test cases throughout this paper.

Fig. 1 lists the different emissive species that may be encountered in this case. Each species is associated with a particular relative quantum yield Φ which will be estimated from the PAM quenching analysis curves. In the appendix it will also be demonstrated for the V and Z preparations how some of these quantum yields can also be independently estimated from picosecond time-resolved fluorescence measurements.

Thus our approach does take into account the biophysical origin of the emitting states which can interconvert, but describes the dynamics phenomenologically, i.e. with exponential decays. In the discussion we will close the loop, and connect to a theoretical model. The predictions from such a model can be quantitatively compared to the results from our parametric description, and thus inspire the iterative improvement of the theoretical model.

2. Materials and methods

The relevant paragraphs of the material and methods section from [17] are reproduced below with minor modifications and clarifications.

2.1. Chloroplasts isolation

Spinach plants were grown for 8–9 weeks in Sanyo plant growth cabinets with an 8-h photoperiod at a light intensity of 250 μmol of photons $m^{-2} s^{-1}$ and a day/night temperature of 22/18 °C. Intact chloroplasts were prepared as described in [21]. Chloroplasts devoid of zeaxanthin and antheraxanthin (labeled -Zea or just V) were prepared from spinach leaves dark adapted for 1 h. Chloroplasts enriched in zeaxanthin (labeled + Zea or Z) were prepared from leaves pretreated for 30 min at 350 μmol of photons $m^{-2} s^{-1}$ under 98% N_2, 2% O_2.

2.2. PAM fluorometry

Chlorophyll fluorescence was measured with a Dual-PAM-100 chlorophyll fluorescence photosynthesis analyzer (Heinz Walz) using the liquid cell adapter. Intact chloroplasts were measured in a quartz cuvette at a concentration of 12 μM chlorophyll under continuous stirring in the presence of 100 μM methyl viologen as a terminal electron acceptor. Actinic illumination (350 μmol of photons $m^{-2} s^{-1}$) was provided by arrays of 635 nm LEDs. Fo (the fluorescence level with PSII reaction centers open) was measured in the presence of a 10 μmol of photons $m^{-2} s^{-1}$ measuring beam (fluorescence emitter: 620 nm (DUAL-DB)). The maximum fluorescence in the dark adapted state (Fm), during the course of actinic illumination (Fm′) and in the subsequent dark relaxation periods was determined using a 0.8 s saturating light pulse (4000 μmol of photons $m^{-2} s^{-1}$). This is a standard protocol of applying saturating light pulses and the 0.8 s duration was chosen not to induce quenching, which was tested on dark-adapted samples subjected to pulses. The Fm level was found to be constant if 500–800 ms pulses were applied [22].

2.3. Time-resolved fluorescence spectroscopy

Time-correlated single photon counting measurements were performed using a FluoTime 200 ps fluorometer (PicoQuant). Fluorescence lifetime decay kinetics were measured on LHCII and intact chloroplasts (4 μM chlorophyll) using excitation provided by a 470-nm laser diode using a 10 MHz repetition rate. These settings were carefully chosen to be far below the onset of singlet-singlet exciton annihilation (< 0.1 pJ). Time-resolved emission spectra (TRES) were measured in the 655–760-nm detection region with 1-nm steps. The resolution of the time-to-amplitude converter was 4 ps/channel.

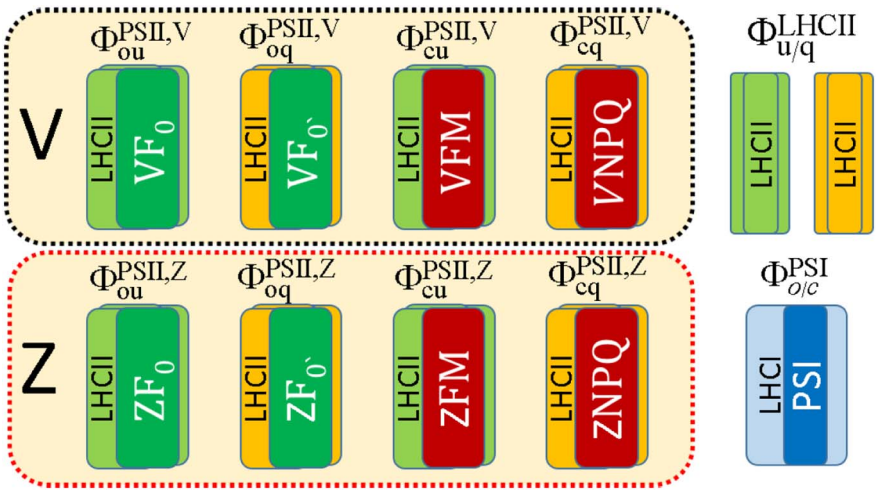

Fig. 1. Overview of the different emissive species that can contribute to a measured PAM curve for plants and green algae. The Photosystem II supercomplex can occur in four different states depending on whether the RC is open (o) or closed (c), and the complex as a whole is being quenched non-photochemically (q) or unquenched (u). The states are duplicated between the two different samples (V, Z) to emphasize that the yields may be different. Photosystem I can contribute but is assumed to be unaffected by quenching or saturating light conditions. Disconnected LHCII can also contribute and is assumed to be affected by quenching in the same way as PSII. Under normal conditions it is only present in negligible amounts.

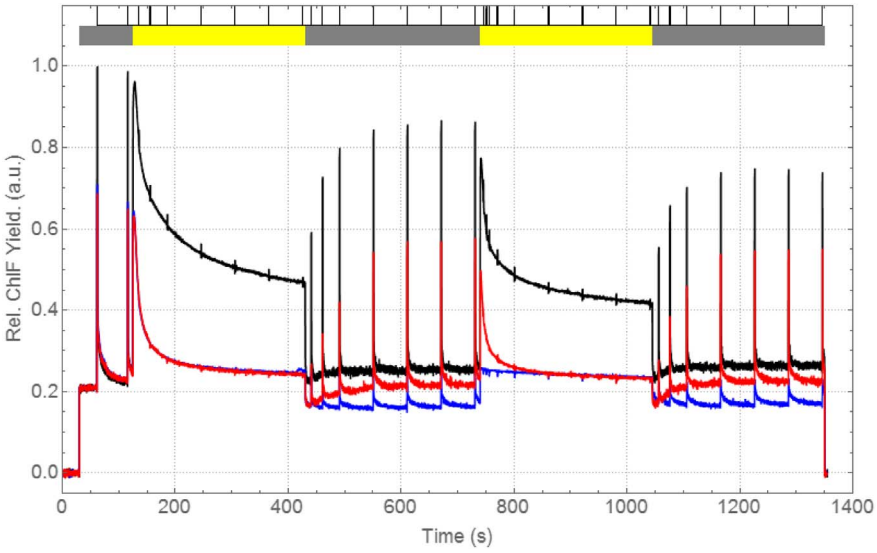

Fig. 2. PAM fluorescence quenching/induction curves obtained on intact Chloroplasts devoid of zeaxanthin (black), enriched in zeaxanthin (red, blue) using the saturating pulse method. Alternating darkness (dark adaptation, recovery, indicated by a gray bar above the curve) and continuous actinic light (inducing quenching, yellow bar) to measure quenching induction/recovery while periodically probing the maximal level of fluorescence with saturating pulses (indicated by stripes in the top of the graph). The blue curve represents a sample where glutaraldehyde was added (at t ≈ 410 s) to prevent the recovery from the quenched state. Its peaks are obscured in this overlay figure, but are clearly visible in **Fig. S7**. The black curve was normalized to the maximum of the fluorescence in darkness, and the red and blue curves were then scaled to the minimal level of fluorescence in darkness of the black curve. Measuring light and actinic light of 620 and 635 nm respectively was used, and fluorescence was detected above 700 nm.

3. Experimental data

Fig. 2 shows three measured PAM fluorescence quenching curves obtained on dark adapted intact spinach chloroplasts either devoid (black curve) of, or enriched in zeaxanthin (red and blue curves), labeled respectively the “V”, “Z” and “GA” dataset. The relative chlorophyll fluorescence quantum yield is probed over a period of 25 min with 60 millisecond sampling intervals while subjected to a complex actinic light protocol controlling the actinic background light and saturating flashes. The GA dataset represented by the blue curve in Fig. 2 is similar to the Z dataset, except that around t ≈ 410 s glutaraldehyde was added, largely inhibiting recovery of quenching. Glutaraldehyde, at the concentration used, stops NPQ recovery in the dark. Not only Fm′ but also Fo′ remains constantly in the quenched state. Delta-pH collapses though but judging by the stable PSII yield, the electron transport around PSII remains unaffected. The same data was presented in Fig. 1A of [17]. The light protocol can be used to distinguish a number of light regimes (LR0–LR6), indicated in the white/gray/yellow bar in Fig. 2. In the first 30 s (LR0: 0.02 s–30.02 s; white) a background signal is measured. Then the measuring light is switched on while the actinic light is still switched off (LR1: 30.08 s–124.94 s; gray), probing the minimal variable fluorescence level in the dark, typically labeled Fo and associated with completely open PSII RCs. Periodically a saturating pulse of light (0.8 s; 4000 μmol m^{-2} s^{-1}) is applied (indicated by a black stripe on top of the bar in Fig. 2) probing the maximal level of variable fluorescence, typically labeled Fm when the sample is dark adapted, and labeled Fm′ while the sample is exposed to actinic light, and associated with completely closed RCs. During the initial period of darkness two such saturating pulses are applied and some recovery dynamics following the saturating pulse is observed. The next phase of the experiment consists of a period of actinic light (level = 350 μmol @ 635 nm) (LR2: 125.0–429.98; yellow) in which fluorescence quenching in the form of a steady decline of the fluorescence yield is observed, followed by a period of darkness (LR3: 429.98–740.0; gray) where the fluorescence (partially) recovers to the levels of the dark adapted state. A second period of actinic light (LR4: 740.06–1045.1; yellow) is again followed by a period of darkness (LR5: 1045.16 s–1350.02 s; gray) showing somewhat different dynamics, before the measurement light is again switched off (LR6: 1350.08 s–1354.94 s, white). Thus, the whole measurement can be divided into a number of discrete segments starting at the moment of a change in light conditions (measuring light on or off, actinic light on or off, saturating pulse on or off) and ending the moment in time just before another change is observed. For these data this amounts to 77 unique segments. The beginning of each segment can be determined from the data by visual inspection, it can be estimated during the analysis, or, ideally, it can be automatically generated from the experimental protocol that was used to record the data. In each segment the data are fitted with a unique model function defined with respect to the start of the segment (time zero; t_0), while all model functions share a common parameter set.

4. Constructing a parametric model

To create a parametric description of our experimental data, we start by recognizing that the experimental data is the result of a PAM fluorometer running a complex light protocol while sampling the fluorescence quantum yield with high resolution. The protocol specifies exactly when and for how long the sample is exposed to a certain intensity (ranging from high to none) of actinic light and additionally when and for how long saturating flashes are given. The signal that is measured depends on the stoichiometry of the species probed with the PAM measuring light, as well as their specific quantum yield which, in the case of PSII, can strongly depend on the actinic light conditions. While the sum of concentrations of species may be constant, their stoichiometry certainly isn't. In this case study we consider four states of PSII: it can be open or closed and it can be part of a quenched or unquenched complex (see Fig. 1). PSII is considered closed when the Q_A site is reduced. We will return to the consequence of ignoring the PSI contribution in the discussion. Fig. 3 summarizes the method of analysis of PAM curves using a parametric model, subsequently every aspect will be discussed in more detail.

In order to construct a parametric model that can be used to fit and quantitatively describe PAM fluorometry curves the following assumptions are made. 1) The total fluorescence quantum yield can be described as the linear combination of the concentrations of a number of emissive species c^j and their quantum yields Φ^j. 2) The quantum yields of these species are independent of their relative concentration or experimental (lighting) conditions.

A species is then defined as a pigment-protein complex which can be excited by the measuring light of the PAM fluorometer and which has a unique spectral and kinetic signature of excited state decay resulting in a specific contribution to the emission in the integration window of the PAM fluorometer (see also Fig. 1). The concentrations of the different species can change dynamically when one species is interconverted into another, in which case the sum of the concentrations can be assumed to remain constant. For instance if the process of closing PSII RCs by applying a saturating pulse can be described with f(t) the concentration of open PSII is described with (1-f(t)). With high light exposure species

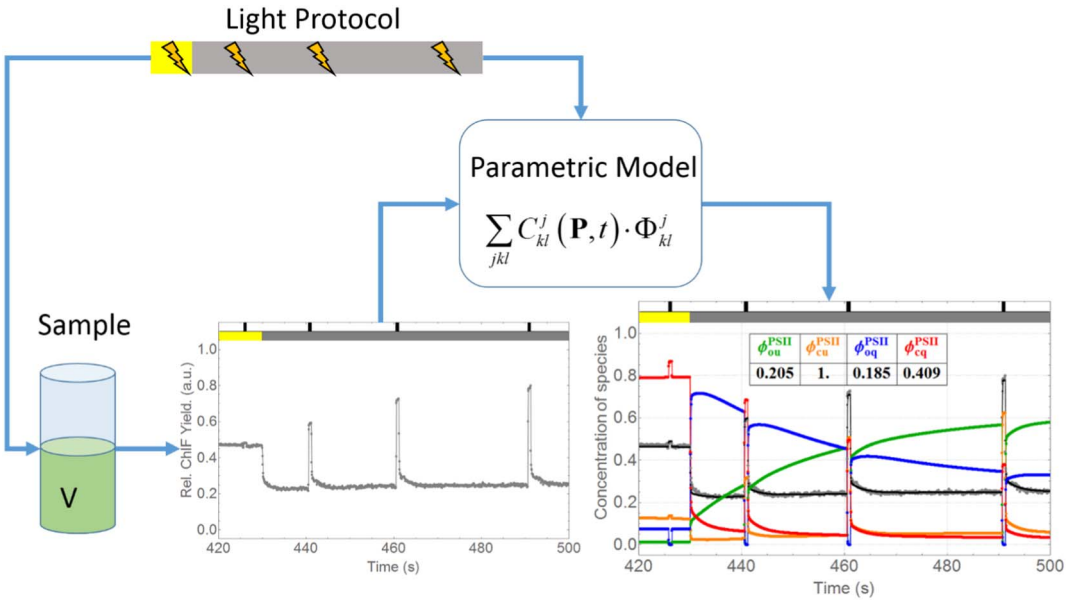

Fig. 3. PAM analysis method using a parametric model. A sample (of in this case intact chloroplasts devoid of zeaxanthin) is measured following a specific light protocol consisting of regimes of quenching inducing continuous actinic light, recovery regimes with no actinic light, and saturating pulses throughout the experiment. The resulting data as well as the light protocol form the input for a parametric model which results in a description of the data in terms of a number of species concentrations c^j and their quantum yields Φ^j.

could get photoinactivated, leading to the photoinhibition of PSII activity. The dynamics of the concentrations as a function of the measurement time C_t is dependent on the light conditions of the experiment and can be parameterized with a parameter vector P, which is independent of the species specific quantum yield Φ.

The total PAM signal J, decomposed into j species, can then be written as:

$$J^{x}(\mathbf{C}_t(\mathbf{P});\Phi)=\sum_{jkl} c_{kl}^{j,x}(\mathbf{P},t)\cdot\Phi_{kl}^{j,x} \tag{1}$$

where the additional indices k and l represent different light–acclimated states; e.g. in the case of PSII k takes into account whether the state is open or closed and l stands for either a quenched or an unquenched species The label x is used to represent the state of zeaxanthin enrichment, e.g. V in the case of a sample devoid in zeaxanthin and Z in the case of the sample enriched in zeaxanthin. Enumerating over all species j for state x (where x equals V or Z) we get:

$$J^{x}=c_{ou}^{\mathrm{PSII,x}}.\Phi_{ou}^{\mathrm{PSII,x}}+c_{cu}^{\mathrm{PSII,x}}.\Phi_{cu}^{\mathrm{PSII,x}}+c_{oq}^{\mathrm{PSII,x}}.\Phi_{oq}^{\mathrm{PSII,x}}+c_{cq}^{\mathrm{PSII,x}}.\Phi_{cq}^{\mathrm{PSII,x}} \tag{2}$$

Taking the assumption of a limited number of discrete states (Fig. 1) substituted into a parametric model (Eq. (1) and Fig. 3) resulting in Eq. (2) we arrive at our working model depicted in Fig. 4. Here the dynamics of the concentrations $c_{ou}^{\mathrm{PSII,x}}, c_{cu}^{\mathrm{PSII,x}}, c_{oq}^{\mathrm{PSII,x}}, c_{cq}^{\mathrm{PSII,x}}$ is captured by a limited number of rate constants (k_1, k_2, etc), reflecting the interconversion of one state in the system to another. For instance k_1 (in a saturating pulse) or k_{10} (under actinic light) reflect the rates in which open unquenched PSII is converted to closed unquenched PSII, subsequently k_4, k_{4a} and k_5 reflect the three rate constants needed to describe the quenching of PSII under the continued influence of actinic light (indicated by a red arrow). Returning to darkness the re-opening of the RC is described by k_2, k_3 and k_{3b} and the recovery from quenching by rates k_8 and k_{8a} which occur in the absence of light as indicated by the blue arrows.

The amplitude fractions (how much decay can be ascribed to a particular rate constant) have been omitted from the figures for the sake of brevity, but are discussed below. Detailed considerations are described in the SI, section "Components of a parametric model for PAM curves", which also lists the complete set of equations used for the total fitting function. To simplify the model, we assume that the concentration of zeaxanthin remains constant throughout the course of the experiment, as adding this complexity would add a third dimension to the model whereas the fitting results show that given the short duration of the experiments this extra complexity is not needed to adequately describe the data.

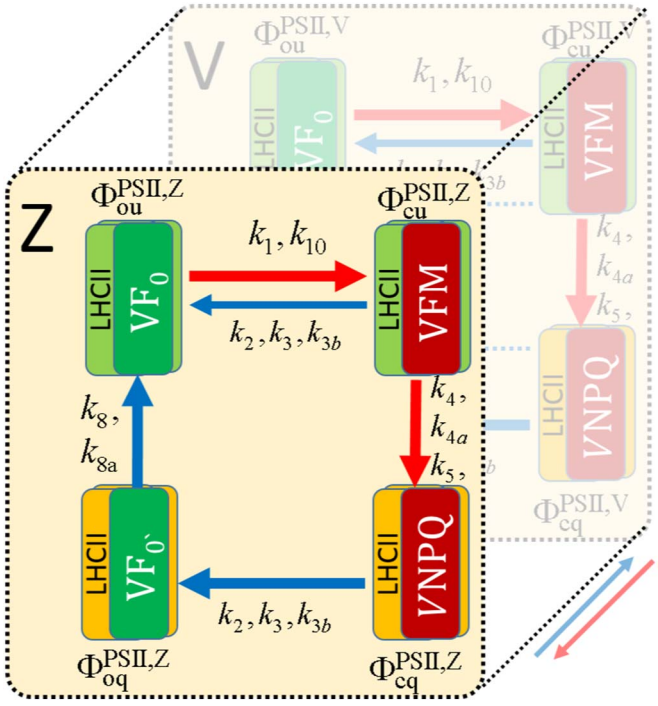

Fig. 4. Working mathematical model which ties the different species listed in Fig. 1 to the parametric description given in Eq. (2). The premise of the model are four distinct states which can be interconverted into one another with certain rates, either light driven (red arrows) or spontaneously in the absence of light (blue arrows). To simplify the model it was assumed that during the course of the experiment the concentration of zeaxanthin remains constant so that species only interconvert within the front plane defined by a certain fixed level of zeaxanthin.

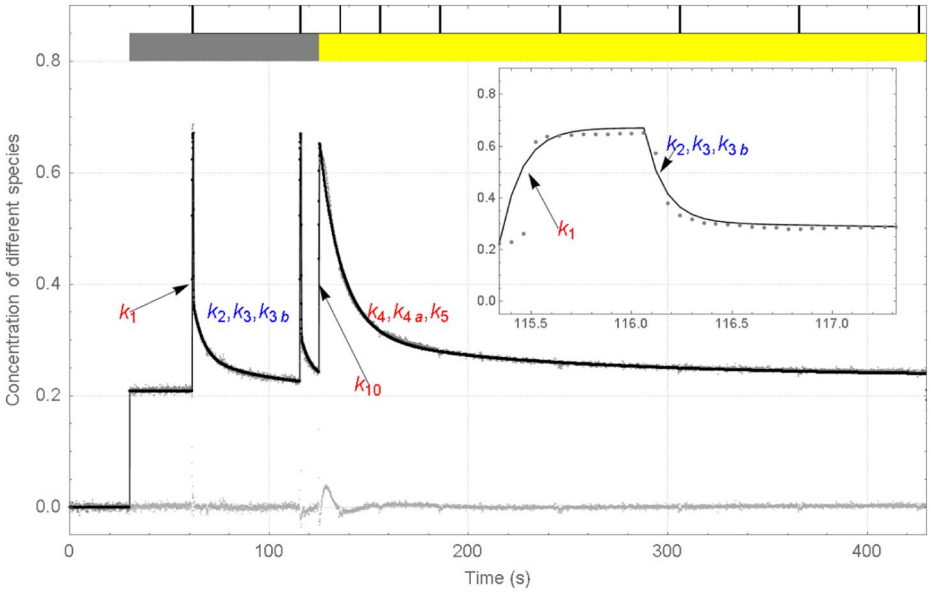

Fig. 5. Simulated PAM curve of intact spinach chloroplasts enriched in zeaxanthin. Legend: data (gray), simulation (black), residual (light gray, straddling the zero line). The bottom half of the color bar indicates the light condition (white: no ML, gray: only ML, yellow: ML and actinic light). The upper half indicates when a SP was applied. The inset represents a zoom of the second saturating pulse in darkness. The inset labels indicate which of the rates k_i from Fig. 4 apply to which segments in the data. Further details are discussed in the text.

5. Simulating PAM fluorometry curves

Using the function definition of Eq. (2) the quenching analysis curves can either be simulated using any chosen set of parameters or fitted directly to the measured data from Fig. 2. To illustrate the different aspects of the model, a simulation is performed with parameters which are in good agreement with those needed to describe the measurements of zeaxanthin enriched chloroplasts (red curve, Fig. 2). See **Fig. S2** for an impression of the implementation of the simulation. Note that in the screenshot the contributions from species other than PSII (e.g. PSI) have been set to zero in this simulation. The first part of the simulation consists of a brief period of darkness, with two saturating pulses, and then a period of quenching inducing high light; this is shown in Fig. 5. The recovery period that follows the period of continuous actinic light is shown in Fig. 6. For comparison the measured data is shown by gray dots and the simulated trace in solid black. The residuals, defined as data minus simulation, are shown in light gray. Given the noise level of the data (standard deviation is < 0.01) it is clear from the residuals of this simulation that the model is not perfect but all essential features of the data *are* captured, which will be discussed below.

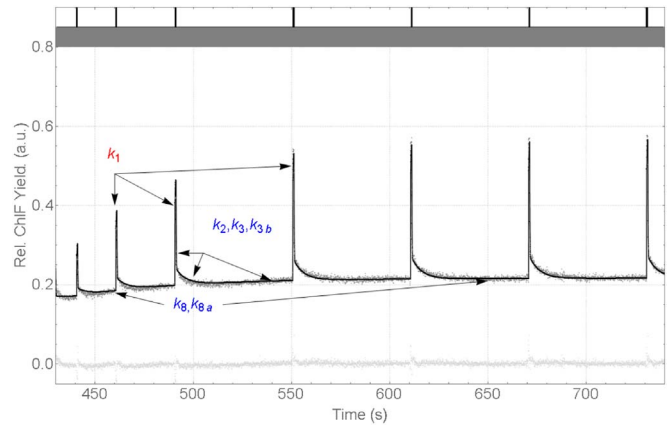

Fig. 6. Simulated PAM curve representing the recovery region following a period of actinic light as in Fig. 5. The simulated trace is in solid black, the observations are represented by dark gray dots. In light gray dots (straddling the zero line) are the residuals. The inset labels indicate which of the rates from Fig. 4 apply to which segments in the data.

The simulation starts with 30 s of background signal (ML off). When the ML is turned on (but the actinic light is still off), the signal instantaneously (in less than the 60 ms step size) reaches a level of minimal variable fluorescence, which can be written as the product of a time dependent (but in this case constant) concentration function and a constant quantum yield (the same throughout the simulation): $J = c_{ou}^{PSII}(t) \cdot \Phi_{ou}^{PSII}$ (where ou indicates that the RC is open and the complex as a whole is unquenched), with in this case $c_{ou}^{PSII}(t) = 1$, $\Phi_{ou}^{PSII} = 0.21$. Note that this quantum yield is not absolute but relative to the chosen normalization in Fig. 2. During this period of relative darkness (only ML) at two moments in time ($t_{SP1} = 61.40$; $t_{SP2} = 115.34$) a saturating pulse of about 0.8 s is applied, which is assumed to quickly close all PSII RCs, but not induce any quenching. This translates to a full conversion of the concentration of open unquenched PSII to closed unquenched PSII. The expression that captures this can be written as:

$J = e^{-k_1}(t - t_0) \cdot \Phi_{ou}^{PSII} + (1 - e^{-k_1}(t - t_0)) \cdot \Phi_{cu}^{PSII}$ where $k_1 = 9.4 s^{-1}$, $\Phi_{ou}^{PSII} = 0.21$ as before, $\Phi_{cu}^{PSII} = 0.67$ and where in lieu of t_0 either t_{SP1} or t_{SP2} is substituted. After the saturating pulse the subsequent reopening of the closed PSII RCs is modeled using a sum of three exponentials that describes the conversion of closed unquenched PSII back into open unquenched PSII.

$J = (1 - c_{cl}^{PSII}(t)) \cdot \Phi_{ou}^{PSII} + c_{cl}^{PSII}(t) \cdot \Phi_{cu}^{PSII}$ with $c_{cl}^{PSII}(t) = a_2 e^{-k_2 D1}(t - t_0) + a_3 e^{-k_3}(t - t_0) + a_{3b} e^{-k_{3b}}(t - t_0)$
where $k_2 = 9.4 s^{-1}, k_3 = 0.002 s^{-1}, k_{3b} = 0.16 s^{-1}$,
$a_2 = 0.65, a_3 = 0.06, a_{3b} = 0.29$ for SP1 and $a_2 = 0.81, a_3 = 0.03$, $a_{3b} = 0.16$ for SP2. The recovery after the very first saturating pulse in darkness is slower than that after subsequent saturating pulses.

Following the period of relative darkness, as indicated by the gray bar in Fig. 3, is a period of continuous actinic light, indicated by a yellow bar. The moment the actinic light is switched on (t_{LR2}) the fluorescence level is observed to rise due to the closing of all PSII RCs, which is again approximated with a single exponential rise. However, the maximum level of fluorescence yield reached is somewhat lower than during the saturating pulses in darkness, which is modelled here by the immediate onset of a fast quenching process. This means that at this point all states of PSII as illustrated in Fig. 1 can occur simultaneously. For simplicity we only describe the contribution of PSII in the closed and quenched state, by far the dominant component during the period of actinic light, which can be written as the product of a closing function and a quenching function times the relevant quantum yield:

Table 1
Parameter values estimated using non-linear regression. Four quantum yields, sixteen rate constants and ten fractional amplitude parameters are given. For more information on the nature of each parameter the reader is referrred to **Table S1** and the corresponding section in the SI. The relation between the fractional amplitude parameters and the amplitude parameters reported in the main text is given in Table S2. Parameters fixed during regression are indicated in bold. Parameters that were not relevant for a given case are marked with '–'. The value of k_8^{R1}listed for the Z + GA case applies to the Z dataset only, for the GA dataset it was fixed to 0 (there is no recovery from quenching in this case).

	Φ_{oq}^{PSII}	Φ_{ou}^{PSII}	Φ_{cq}^{PSII}	Φ_{cu}^{PSII}	k_1^{D1}	k_1^{H1}	k_{10}^{H1}	k_2^{D1}	k_{3b}^{D1}	k_3^{D1}
V	**0.185**	0.205	0.409	**1.000**	20	20	9.3	16	0.41	0.0441
Z	0.152	0.209	0.234	0.671	9.5	–	11	9.9	0.19	0.0238
GA	0.159	0.207	0.231	0.701	9.4	–	24	9.5	0.16	0.021
Z + GA	0.162	0.209	0.233	0.684	9.5	–	13	9.8	0.19	0.0244

	k_2^{H1}	k_4^{H1}	k_{SQ}^{H1}	k_5^{H1}	k_4^{H2}	k_5^{H2}	k_6^{H1}	k_6^{H2}	k_8^{R1}	k_{8a}^{R1}
V	35	0.050	0.0041	0.132	0.14	0.02	0.027	k_6^{H1}	0.038	0.0002
Z	–	0.008	0.061	0.105	0.02	0.21	–	–	0.020	0.0005
GA	–	0.089	0.0052	**0.1**	–	–	–	–	**0**	0.0005
Z + GA	–	0.006	0.048	0.12	0.02	0.20	–	–	0.019	0.0002

	fr_{CC}^{H1}	fr_{SQ}^{H1}	fr_2^{D1}	fr_{3b}^{D1}	fr_2^{SP1}	fr_{3b}^{SP1}	fr_2^{R2}	fr_{3b}^{R2}	fr_4^{H1}	fr_4^{H2}
V	0.91	0.46	0.81	0.53	0.78	0.54	0.75	0.52	0.77	0.78
Z	1.00	0.27	0.79	0.73	0.66	0.62	0.75	0.64	0.22	0.24
GA	1.00	0.14	0.81	0.73	0.66	0.65	0.39	0.80	0.93	0.24
Z + GA	1.00	0.28	0.80	0.75	0.66	0.62	0.73	0.68	0.18	0.24

$$J_{cq}^{PSII} = \overbrace{(cl_D + (1 - cl_D)(1 - e^{-k_{10}(t-t_0)}))}^{\text{closing}} \overbrace{(1 - fr_{SQ} e^{-k_{SQ}(t-t_{pLR})} - (1 - fr_{SQ})(a_4 e^{-k_4(t-t_{pLR})} + (1 - a_4) e^{-k_5(t-t_{pLR})}))}^{\text{quenching}} \Phi_{cq}^{PSII}$$

Here $cl_D = 0.09$ represents a fraction of the total PSII population which is (still) closed, due to the remaining effect of a preceding saturating pulse, and defined as the function c_{cl}^{PSII} evaluated at the last time point in darkness. The conversion of PSII in the open state to the closed state occurs with a rate of $k_{10} = 10/s$, and t_0 is substituted with the start of the actinic light regime ($t_{LR2} = 125$ s). Quenching is divided into two fractions which differ in their rate of recovery. A slow-to-recover quenching fraction $fr_{SQ} = 0.27$ rises with a rate $k_{SQ} = 0.07\ s^{-1}$. A quick-to-recover fraction $(1 - fr_{SQ}) = 0.73$ rises on two timescales, a small fraction $a_4 = 0.22$ rises relatively slowly with a rate of $k_4 = 0.01/s$ and a fraction $(1 - a_4) = 0.78$ rises with rate $k_5 = 0.1/s$. The full expression can be found in the SI, but in principle it is easily derived since the concentration of PSII in the open state is $(1 - closed)$, and the amount of unquenched PSII is $(1 - quenched)$. The full expression also takes into account that a fraction of the PSII re-opens during the course of actinic light illumination, when the excitation pressure from the actinic light is not enough to keep all PSII RCs closed. In this simulation it is assumed that all RCs are continually closed ($fr_{CC} = 1$, see SI) during actinic light because of the absence of a fluorescence increase upon a saturating pulse during the period of actinic light.

After a period of actinic light follows a period of darkness during which the sample can recover from quenching as shown in Fig. 6. The initial effect of switching from actinic light to relative darkness is re-opening of the PSII RCs, exactly as would happen after a saturating pulse. Then on a longer timescale the sample also recovers from the quenching induced by the actinic light, a fraction recovering quickly and the rest so slowly that at the end of the recovery period a large part of it still hasn't recovered, as can be observed in Fig. 2. For simplicity we describe here only the contribution of PSII in the open unquenched state, which describes the baseline level during a recovery period. Again the other contributions can easily be derived from this expression but for the complete expression the reader is referred to the SI. The contribution of PSII in the open and unquenched state to the total PAM signal J during recovery then becomes:

$$J_{ou}^{PSII} = \overbrace{(a_2(1 - e^{-k_2(t-t_0)}) + a_3(1 - e^{-k_3(t-t_0)}) + a_{3b}(1 - e^{-k_{3b}(t-t_0)}))}^{\text{opening}} \left(\overbrace{(1 - fr_{SQ})(1 - QT_f + (1 - e^{-k_8(t-t_{pLR})})QT_f)}^{\text{fast recovery}} + \overbrace{fr_{SQ}(1 - QT_s + (1 - e^{-k_{8a}(t-t_{pLR})})QT_s)}^{\text{slow recovery}} \right) \Phi_{ou}^{PSII}$$

where $k_2 = 9.4 s^{-1}$, $k_3 = 0.16 s^{-1}$, $k_{3b} = 0.002 s^{-1}$, $a_2 = 0.81$, $a_3 = 0.13$, $a_{3b} = 0.06$, $fr_{SQ} = 0.27$. The variables QT_f and QT_s represent how much quenching was induced during the preceding period of actinic light for the fast-to-recover fraction and the slow-to-recover fraction respectively. In this simulation $QT_f \approx 1$, $QT_s \approx 1$. The rates $k_8 = 0.02/s$ and $k_{8a} \approx 1/h$ are the rates of recovery for the fast and slow fraction respectively. The parameters a_2, k_2, a_3, k_3, a_{3b}, k_{3b}, in principle are linked between the initial period of darkness and the period of recovery, meaning that the dynamics of re-opening, following a saturating pulse in darkness or actinic light, or the re-opening after switching off the actinic light, is treated in the same way.

In general linking the parameters between the different segments is an a priori assumption that fits well, however in the case that the dynamics are clearly observed to be different, additional labeled parameters can be introduced, e.g. k_2^{R1} where the label R1 indicates that the parameter is defined specifically for the first recovery regime. In the same way D1 can be used for the first period of darkness, H1 for the first period of actinic light, H2 for the second, etc.

The values of the estimated parameters, i.e. four estimated quantum yields, sixteen rate constants and ten amplitude fractions are collated in Table 1. Thus with the help of our parametric model we have successfully extracted ≈ 30 parameters from each PAM trace that consisted of 22,583 data points.

6. Calculating derived quantities

With a completely parameterized description of the PAM curve in place, it is possible to calculate derived quantities such as the commonly used NPQ parameter (see **Fig. S3**) however the interpretation of this quantity and especially the fitting thereof is not without controversy [23]. Thus, it is more interesting to directly visualize the individual contribution of each species (or in this case, each state of PSII) to the total signal. This decomposition is visualized for the Z dataset in

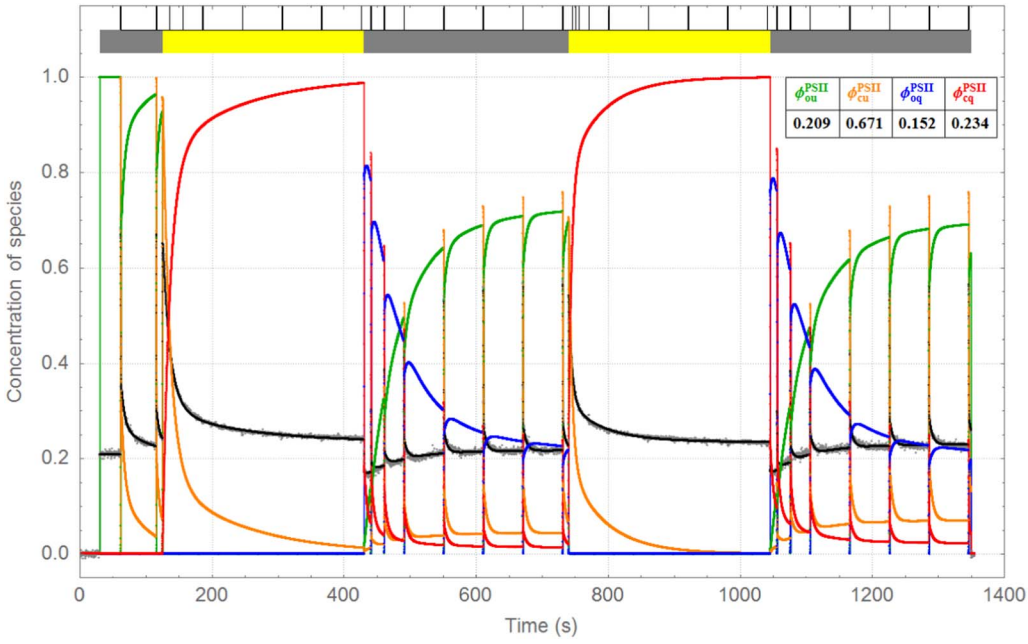

Fig. 7. Concentration profiles of the different states of PSII contributing to the total relative chlorophyll fluorescence quantum yield for the Z dataset. The sum of the concentrations, open unquenched PSII (green, $\Phi_{ou}^{PSII} = 0.209$), closed unquenched PSII (orange, $\Phi_{cu}^{PSII} = 0.671$), open quenched PSII (blue, $\Phi_{oq}^{PSII} = 0.152$) and closed quenched PSII (red, $\Phi_{cq}^{PSII} = 0.234$) multiplied by their respective quantum yields result in the fitted PAM curve depicted in solid black. For comparison the Z observations are overlaid as gray dots. Light conditions are indicated by the top bar as described in the caption of Fig. 2.

Fig. 7 and **Fig. S5**. In Fig. 7 the *concentrations* of the four different states of PSII are shown as a function of the measurement time, at any given moment summing up to a total concentration of 1. In **Fig. S5** the *contribution* of each state to the total quantum yield (overlaid in gray dots, maximum 0.69) is shown. The black curve represents the sum over the product of concentration and quantum yield for all four states (see table inset).

In the beginning, the contribution of PSII open unquenched (green curve) is maximal. At the first saturating pulse this concentration drops to zero and the contribution of PSII in the closed unquenched state (depicted in orange) is maximal. After the saturation pulse is completed (0.8 s after the onset) the concentration of closed unquenched decays back into open unquenched. Just before the next saturating pulse the level is still not yet at the level of Fo in darkness indicating that a small fraction ($\approx 5\%$) is still closed. When the actinic light is switched on (indicated by a yellow bar) the concentration of PSII closed quenched is observed to quickly rise (red curve) at the expense of the closed unquenched state. After switching the actinic light off again the fourth species enters, open quenched PSII (blue curve). The lowest level in the data (well below Fo in darkness) largely determines Φ_{oq}^{PSII}. During the recovery from quenching the quenched concentrations (red/blue) are gradually replaced by unquenched (orange/green), but not completely. A substantial amount ($\approx 20\%$) of open quenched PSII (blue) remains, even after 300 s of recovery. This is a direct consequence of the observation in the data (cf. the red curve in Fig. 2) that the level of Fm′ at the end of the recovery period is substantially lower than Fm in darkness. The same holds true for the maximum level reached upon turning on the actinic light after the first recovery period. This accumulation of a slow-to-recover quencher is described by the remaining concentration in the blue curve. But despite this incomplete recovery from quenching, the baseline level of fluorescence in the data is even slightly higher than the level of F_0 in the initial period of darkness. Considering that the yield of open quenched PSII lies below that of open unquenched PSII, there has to be a certain fraction of closed quenched and closed unquenched PSII left which is seen as a non-zero amplitude of the red and orange curves toward the end of the recovery periods. This permanently closed fraction visible in Fig. 7 is 7% after the first recovery period, and 11% after the second period of actinic light. This effect is even more clearly visible in the decomposition of the V dataset, shown in Fig. 8 (*concentrations*) and **Fig. S6** (*contributions*), where the baseline level of F_0 following a period of recovery is substantially higher than during the initial period of darkness, and the accumulation of the slow-to-recover quencher and the fraction of permanently closed PSII is even more pronounced. Here the permanent closed fraction is 8% after the first recovery period, 17% after the second recovery period.

The main difference between Figs. 7 and 8 is the re-opening of a small fraction of PSII RCs during actinic light. This is directly observed in the data as well: during actinic light upon application of a saturating pulse the observed yield is slightly higher still. This is now visualized in Fig. 8 as the blue concentration, which slowly rises (it is assumed that the initial switching on of the actinic light first closes everything) and which drops to zero every time a saturating pulse is applied. As a consequence the concentration of red/orange features a small spike which lasts only for the duration that the saturating pulse is applied. In contrast to the period of darkness and recovery, where the actinic light is on, the decay of the extra closed concentration is extremely fast under the influence of actinic light. Another relevant difference is that the quenching level reached after the second period of actinic light is substantially lower than after the first period, which is explained by a quenched fraction which takes longer to form and is slow-to-recover.

The decomposition of the GA dataset is shown in **Fig. S4** (concentrations) and **Fig. S7** (contributions).

7. Fitting PAM curves

Instead of mimicking the data by adjusting the parameters by hand, the parameters can also be estimated using any non-linear regression method. The implementation in this paper was constructed in Wolfram Mathematica, but the expression could easily be ported to any other language or platform which has non-linear solvers available, such as Matlab, Python, R or C++.

Fig. 9 shows the fitted PAM curves for the V and Z datasets following optimization of the parameters using non-linear regression. The V data is plotted in gray dots, the fit in solid black, and the residual light gray. The Z data is shown in orange dots, the fit in solid red and the residuals in dark gray.

Not all parameters were set to be free parameters of the fit. In the case of the V dataset the quantum yield of PSII in the closed unquenched state is fixed to 1 by definition, since the data was normalized to the maximum of the first saturating pulse, where the only contribution is assumed to be closed unquenched PSII. In the Z dataset, because the saturating pulses during actinic light don't result in an

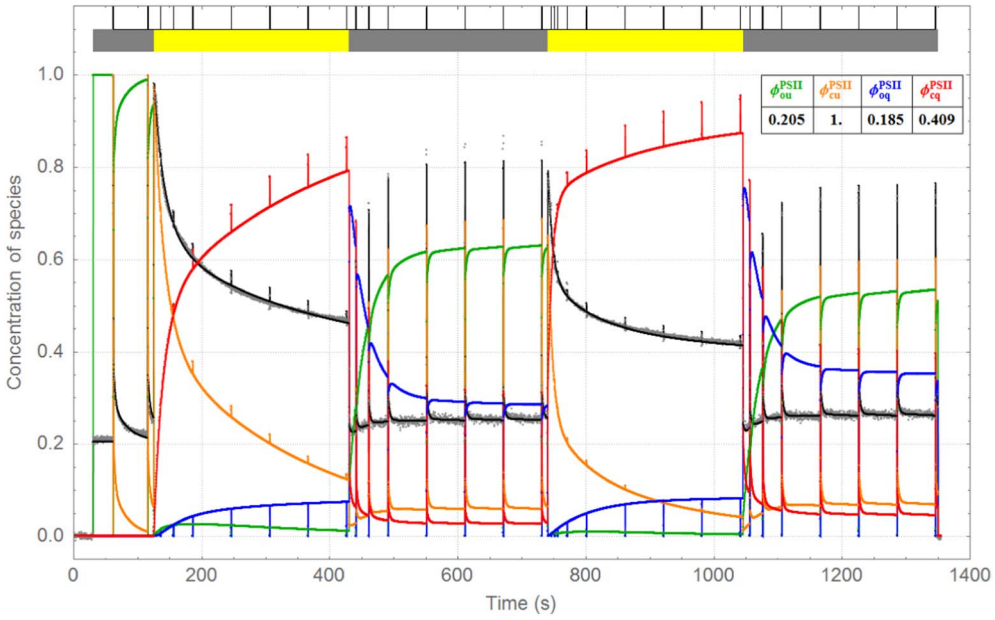

Fig. 8. Concentration profiles of the different states of PSII contributing to the total relative chlorophyll fluorescence quantum yield for the V dataset. The sum of the concentrations, open unquenched PSII (green, $\Phi_{ou}^{PSII} = 0.205$), closed unquenched PSII (orange, $\Phi_{cu}^{PSII} = 1.0$), open quenched PSII (blue, $\Phi_{oq}^{PSII} = 0.185$) and closed quenched PSII (red, $\Phi_{cq}^{PSII} = 0.409$) multiplied by their respective quantum yields produce the PAM curve depicted in solid black. For comparison the V observations are overlaid as gray dots. Light conditions are indicated by the top bar as described in the caption of Fig. 2.

increased yield, the parameter relating to the amount of continuously closed PSII in actinic light (fr_{CC}) was fixed to 1, which automatically means that the rate constant related to partial re-opening (k_6) could be eliminated from the list of parameters to be optimized. Instead in the V dataset the fraction was a free parameter of the fit and could be fitted ($fr_{CC} = 0.9$), and the rate of partial re-opening was found to be $k_6 = 0.03s^{-1}$. In addition it was found that the fraction of slow-to-recover quenching (fr_{SQ}^{H1}) was found to be substantially larger in the V dataset (0.46) than in the Z dataset (0.27) (see Table 1). It is this large value of fr_{SQ}^{H1} which explains the relatively large difference between Fm during the initial phase of darkness (1.0) and Fm′ at the end of the second recovery phase (Fm′ = 0.75), and at least partially the difference between Fm′ at the end of the second and the first period of recovery (Fm′ = 0.85). Recently, a similar slow to recover quenching effect was attributed to plant 'memory' [16], although there it was primarily related to the accumulation of zeaxanthin.

In Fig. 9, the parameters for the V and Z dataset were optimized for each dataset separately, but the real power of having a parameterized description of the PAM curve is when multiple datasets are analyzed with a shared set of parameters, i.e. global analysis of PAM fluorometry data. A straightforward application is when several repeats of a specific protocol are measured on the same sample. Rather than averaging the repeated measurements, they could all be analyzed with a single model with a shared set of parameters. These parameters can thus be estimated more precisely. A more interesting example is to link parameters between different experiments, for instance in the case of the Z dataset, and the GA dataset, which are very similar up to the point where glutaraldehyde is added to the sample in the GA dataset to prevent recovery. To fit both datasets simultaneously a new model function is defined where all parameters are linked between both datasets, except for the rate of recovery for the slow- and fast-to-recover fractions. The rate of fast-to-recover quenching k_8 is set to zero for the GA dataset, whereas the rate of slow-to-recover quenching $k_{8a}$is a free parameter of the fit.

Fig. 10 shows the results of the linked analysis of the Z and GA datasets. Looking at the fitted curves and the residuals in Fig. 10 it is clear that a small price is paid by linking all but one model parameter (k_8, the rate of fast recovery), but overall both datasets are described well with this single model with linked parameters. As more parameters are unlinked (thereby increasing the number of free parameters) the fit

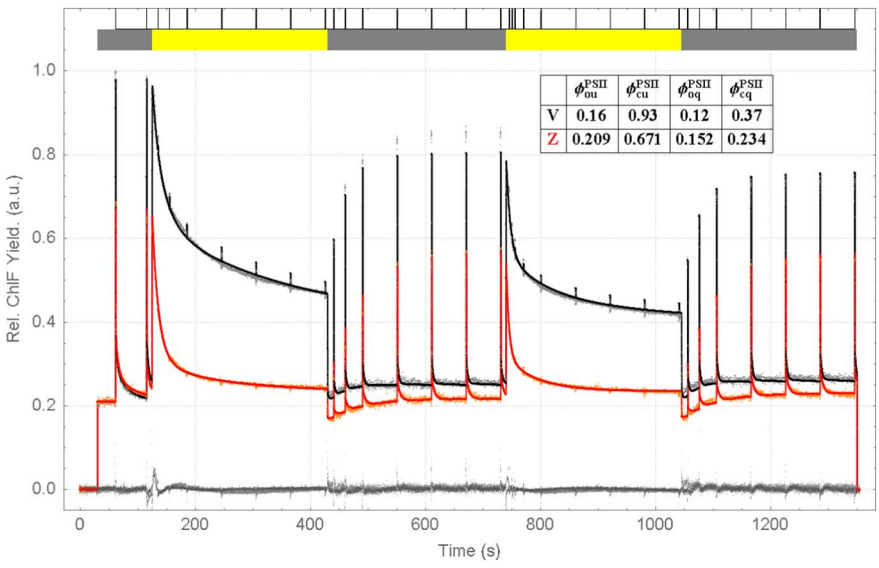

Fig. 9. Fitted PAM curves for the V and Z dataset where non-linear regression was used to estimate the parameters (estimated values in Table 1). Estimated relative quantum yields (relative to$\Phi_{cu}^{PSII,V} = 1$) collated in the inset table. Data, fit and residuals (straddling the zero line) for the V and Z dataset respectively shown in: gray dots, solid black, light gray dots, and orange dots, solid red and dark gray dots. Light conditions indicated by the top bar as described in the caption of Fig. 2.

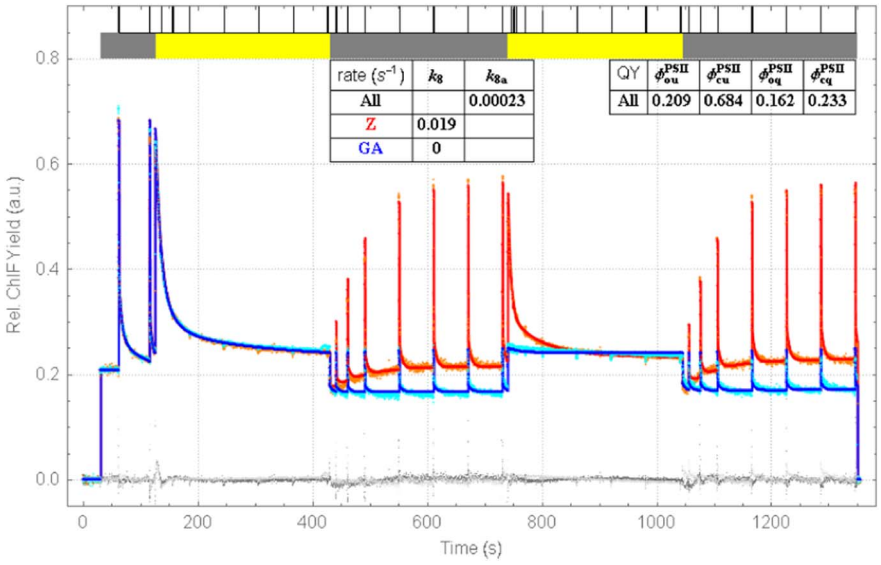

Fig. 10. Simultaneous linked analysis of the Z and GA datasets. The Z data is shown in orange dots, the fit in solid red and the residuals in dark gray. The GA data is plotted in cyan dots, the fit in solid blue, and the residuals in light gray. All model parameters between the two datasets are linked and shown in Table 1except for the rates of slow and fast recovery (shown in the left table inset). The quantum yields estimated from the linked analysis are shown in the right table inset.

can improve. Judging from the values in Table 1 it can also be observed that the linked parameters related to quenching resemble those estimated when fitting the Z dataset alone. For instance the parameter for the fraction of slow quenching (fr_{SQ}^{H1}) is estimated to be 0.27 for the Z dataset, 0.14 for the GA dataset, but 0.28 for the Z + GA linked analysis. Thus the Z dataset contributes relatively more information in the linked fit.

8. Discussion

The key assumption made in this paper is that the fluorescence quantum yield as measured by PAM fluorometry can be described by the sum of a number of discrete molecular states, each with their own fluorescence quantum yield. This assumption derives from the extensive study of photosynthetic samples using time-resolved fluorescence spectroscopy where it can be shown that the observed fluorescence can also be decomposed in the contributions by different complexes [24] facilitated by sophisticated target analysis [25]. We demonstrate that the quantum yields estimated from the analysis of the PAM data are consistent with the quantum yields estimated from ultra-fast time-resolved fluorescence spectroscopy data, see Table S4 in the Supporting Information section “The link with time-resolved fluorescence spectroscopy”. The fact that our model can describe the data without any detachment of the LHCII antenna from PSII is in agreement with the claims of recently published experimental work [26]. Using millisecond fluorescence induction of dark adapted intact chloroplasts [26] discovered that NPQ does not decrease the rate of the transition from Fo to Fm state upon illumination – evidence that the functional antenna size did not decrease in the NPQ state.

Our modelling enabled to assess the amount of photoinactivation based upon the levels of F_0 and F_0'. This assessment is entirely consistent with the recently proposed methodology of the determination of the photoprotective effectiveness of NPQ [27,28]. This photoinactivation assessment methodology uses the relationship between the PSII yield and NPQ as well as compares the measured level of Fo′ and the theoretically predicted Fo′. The parametric model also uses the level of Fo′ to calculate the fraction of the damaged PSII RCs.

Although PSI is part of our parametric model specification and its quantum yield is also estimated in the time-resolved measurements, we have chosen not to include it in the main text/figures for two reasons: (1) PSI contributes only a constant offset as its quantum yield is not significantly affected by the actinic light conditions, therefore it will not affect the estimated dynamics and (2) the results from our analysis of time-resolved fluorescence show the contribution of PSI to be rather small, on the order of 4% of F_m or 20% at F_o (given 475 nm excitation, assuming 1:1 stoichiometry of PSII:PSI). This justifies neglecting the contribution of PSI in first approximation if we're only interested in comparing the relative effect in PSII, but it does signify the importance of a parametric model based analysis which can account for the influence of PSI when it is needed, especially considering the effect on the estimated relative quantum yields. The resulting decomposition including PSI is shown in Fig. S8 (*concentrations*) and Fig. S9 (*contributions*).

Another strong assumption that we have made is that the number of species stays constant throughout the measurement, especially with respect to the sample devoid of zeaxanthin (V sample). In reality the chloroplasts in this sample might accumulate some zeaxanthin throughout the measurement, which has recently been demonstrated to function as a short-term light memory in plants [16]. This would imply that the population dynamics of PSII would have to be modelled with a total of eight species (present in the inset table of Fig. 9). This would be in agreement with the so called four state two site quenching description of PSII [16,29], which attributes the fast induced quenching to a mechanism driven by the pH sensing protein PsbS and the slower quenching to the formation of zeaxanthin [21,30,31]. However, despite our simplification to only four states for PSII per measurement, we have demonstrated an overall good agreement with the data.

In order to facilitate the comparison between our approach and the theoretical model by Matuszyńska et al. we have used our light protocol in their simulation code and generated a comparable decomposition (see Fig. S12). In their model Matuszyńska et al. take into account a fraction of open and closed PSII and a total level of quenching dependent on the relative concentrations of PsBs and Zeaxanthin. This amounts to a gradually increasing level of quenching of all PSII RC's, rather than a gradual population switch between unquenched and quenched centers as is the case in our model. The comparison between our V dataset and the prediction of Fig. S12 shows that although there is reasonable qualitative agreement much of the dynamics is not yet captured. The analysis of Fig. 8 can inspire the iterative improvement of the theoretical model. In particular, a fraction of slowly recovering closed unquenched seems necessary to describe the F_0' deviations in Fig. S12.

Fluorescence quenching analysis by means of PAM fluorometry is a useful tool to study NPQ in different samples under a wide variety of physiologically relevant conditions. In one experiment the information about the condition of the sample before illumination, during quenching inducing continuous actinic light and during recovery can be obtained (Fig. 2). Underlying the fluorescence quantum yield measured

by the PAM fluorometer are the contributions from a number of different emissive species, summarized in Fig. 1 for the case of plants. Each species corresponds to a pigment-protein complex with its own concentration and its own absorption and emission signature for the combination of excitation by the PAM instrument measuring light and its detection window. This simple observation is enough to then formulate Eq. (1) which states that the observed PAM signal can be parametrized as the sum of a number of species' concentrations multiplied by their quantum yields (Fig. 3). Even for a typical PAM analysis quenching experiment as depicted in Fig. 2, the concentration function can get complicated rather quickly, because the concentration of each species is not only dependent on the light conditions at time *t*, but also on the light conditions at all times prior to this. By segmenting the dataset based on changes in the light condition experienced by the sample, either due to the presence or absence of measuring light or the presence or absence of actinic light, and observing which segments preceded, it becomes possible to describe the dynamics for each segment with a limited number of functions (see **Table S1**). In principle the segmentation can be entirely automated if the PAM measurement protocol is known, although the start and end time point for each segment can also be determined empirically from the data, either by manual inspection or by fitting it. Each function is composed of a number of basis functions from a so called Basis Function Set as detailed in the section “Components of a parametric model for the PAM curves” in the SI. For this paper the aim was to keep the function description as simple as possible, so all concentration dynamics is essentially described by a number of exponential functions (for the rise and decay) and a constant term (to reflect the transitional effects). For instance the closing of PSII RCs due to the application of a saturating pulse is modelled by a single exponential rise (thus the concentration of open PSII RCs, defined as one minus the concentration of closed PSII RCs is modeled by a single exponential decay). From the inset of Fig. 5 it can be seen that this is not a perfect description of the observed rise, but it captures the trend and more importantly the starting and end concentration are modelled correctly. It is known from the literature that this fluorescence induction dynamics is much more complex than can be captured by a single exponential rise, and many papers have been published that model this dynamics in great detail (e.g. [32,33]. reviewed in [34,35]). It was shown that when data is obtained at a higher time-resolution at least 3 exponentials are needed [6,36], in which case it would be worthwhile to extend the Basis Function Set to capture this dynamics, but for the datasets used in this work only 13 data points are observed during a saturating pulse and a single exponential sufficed. Overall it can be seen from Figs. 5 and 6 that with the limited set of functions described in **Table S1** the data can be mimicked quite accurately. Of course with a full parameterized description of the PAM curve it is also possible to gain more insight in the closing and quenching dynamics by overlaying the data with the concentration profiles of the individual species as shown in Fig. 7; the sum of the products of the quantum yields (inset) and their concentrations then reproduce the observed PAM fluorescence quantum yield (cf. Eq. (1)). A parameterized description allows for the use of standard non-linear regression to estimate the parameters from the data as is demonstrated in Fig. 9 for the V and Z datasets. But the real power of a parametrized description is revealed when multiple datasets are fitted simultaneously with a common set of parameters. The simplest application of this is when instead of averaging several measurements on the same sample, the measurements are analyzed with a single model resulting in statistically relevant quantities with a meaningful standard deviation. This can be done *even* when there is a small shift in the exact time of the saturating pulses or of the moment of switching on the actinic light between measurements, which would significantly distort the averaged data. A more advanced application is shown in Fig. 10 where the Z and the GA measurements, with at first sight completely different dynamics, are simultaneously fitted with a common set of parameters and only a *single* free parameter between the two datasets. In this way the hypothesis of what exactly happens to the quenching dynamics upon the addition of glutaraldehyde can be more rigorously tested. The fitted parameters obtained by fitting each dataset individually, as well as the parameters obtained in the combined fit, are listed in Table 1. These results demonstrate that the analysis of a single PAM fluorometry quenching experiment can already provide information on the relative quantum yield of the four different states of PSII for the intact chloroplasts. To the best of our knowledge no other form of spectroscopy provides this information in a single measurement.

Transparency document

The http://dx.doi.org/10.1016/j.bbabio.2017.08.004 associated with this article can be found, in online version.

Acknowledgments

This research is performed as part of the BioSolar Cells research programme, sponsored by the Dutch Ministry of Economic Affairs. IHMvS and RvG acknowledge financial support of the European Research Council (Advanced Grant Proposal 267333 (PHOTPROT) to RvG). RvG gratefully acknowledges his Academy Professor grant from the Netherlands Royal Academy of Sciences (KNAW). AVR acknowledges the Leverhulme Trust grant RPG-2012-478 and UK Biotechnology and Biological Sciences Research Council grant BB/L019027/1. AVR would like to acknowledge The Royal Society for the Wolfson Research Merit Award and the NWO visiting scholarship grant 040.11.433. MPJ would like to acknowledge the Leverhulme Trust grant ECF-2012-398\2. JM Gruber and LW Bielczynski are thanked for helpful discussions regarding the interpretation of the modeling.

Appendix A. Supplementary data

Supplementary data to this article can be found online at http://dx.doi.org/10.1016/j.bbabio.2017.08.004.

References

[1] A.V. Ruban, Nonphotochemical chlorophyll fluorescence quenching: mechanism and effectiveness in protecting plants from photodamage, Plant Physiol. 170 (2016) 1903–1916.
[2] J. Kromdijk, K. Głowacka, L. Leonelli, S.T. Gabilly, M. Iwai, K.K. Niyogi, S.P. Long, Improving photosynthesis and crop productivity by accelerating recovery from photoprotection, Science 354 (2016) 857–861.
[3] U. Schreiber, Pulse-amplitude modulation (PAM) fluorometry and saturation pulse method: an overview, Chlorophyll a Fluorescence: A Signature of Photosynthesis, 2004, pp. 279–319.
[4] U. Schreiber, U. Schliwa, W. Bilger, Continuous recording of photochemical and non-photochemical chlorophyll fluorescence quenching with a new type of modulation fluorometer, Photosynth. Res. 10 (1986) 51–62.
[5] W. Bilger, U. Schreiber, M. Bock, Determination of the quantum efficiency of photosystem II and of non-photochemical quenching of chlorophyll fluorescence in the field, Oecologia 102 (1995) 425–432.
[6] W.J. Vredenberg, A three-state model for energy trapping and chlorophyll fluorescence in photosystem II incorporating radical pair recombination, Biophys. J. 79 (2000) 26–38.
[7] R.J. Ritchie, Fitting light saturation curves measured using modulated fluorometry, Photosynth. Res. 96 (2008) 201–215.
[8] G. Schansker, S.Z. Tóth, L. Kovács, A.R. Holzwarth, G. Garab, et al., Biochim. Biophys. Acta Bioenerg. 1807 (2011) 1032–1043.
[9] D. Lazár, G. Schansker, Models of chlorophyll a fluorescence transients, Photosynth. Silico 29 (2009) 85–123.
[10] A. Rubin, G. Riznichenko, Govindjee, Modeling of the primary processes in a photosynthetic membrane, in: A. Laisk, L. Nedbal (Eds.), Photosynthesis In Silico: Understanding Complexity from Molecules to Ecosystems, Springer, Netherlands, 2009, pp. 151–176.
[11] N. Belyaeva, A. Bulychev, G.Y. Riznichenko, A. Rubin, Thylakoid membrane model of the Chl a fluorescence transient and P700 induction kinetics in plant leaves, Photosynth. Res. (2016) 1–25.
[12] O. Ebenhöh, T. Houwaart, H. Lokstein, S. Schlede, K. Tirok, A minimal mathematical model of nonphotochemical quenching of chlorophyll fluorescence, Biosystems 103 (2011) 196–204.
[13] J. Zaks, K. Amarnath, D.M. Kramer, K.K. Niyogi, G.R. Fleming, A kinetic model of rapidly reversible nonphotochemical quenching, Proc. Natl. Acad. Sci. 109 (2012)

15757–15762.
[14] O. Ebenhöh, G. Fucile, G. Finazzi, J.-D. Rochaix, M. Goldschmidt-Clermont, Short-term acclimation of the photosynthetic electron transfer chain to changing light: a mathematical model, Philos. Trans. R. Soc. Lond. B Biol. Sci. 369 (2014) 20130223.
[15] A. Matuszyńska, O. Ebenhöh, A reductionist approach to model photosynthetic self-regulation in eukaryotes in response to light, Biochem. Soc. Trans. 43 (2015) 1133–1139.
[16] A. Matuszyńska, S. Heidari, P. Jahns, O. Ebenhöh, A mathematical model of non-photochemical quenching to study short-term light memory in plants, Biochim. Biophys. Acta Bioenerg. 1857 (2016) 1860–1869.
[17] M.P. Johnson, A.V. Ruban, Photoprotective energy dissipation in higher plants involves alteration of the excited state energy of the emitting chlorophyll(s) in the light harvesting antenna II (LHCII), J. Biol. Chem. 284 (2009) 23592–23601.
[18] R.B. Peterson, V. Oja, H. Eichelmann, I. Bichele, L. Dall'Osto, A. Laisk, Fluorescence F_0 of photosystems II and I in developing C_3 and C_4 leaves, and implications on regulation of excitation balance, Photosynth. Res. 122 (2014) 41–56.
[19] G. Schansker, S.Z. Tóth, R.J. Strasser, Methylviologen and dibromothymoquinone treatments of pea leaves reveal the role of photosystem I in the Chl a fluorescence rise OJIP, Biochim. Biophys. Acta Bioenerg. 1706 (2005) 250–261.
[20] E. Belgio, M.P. Johnson, S. Jurić, A.V. Ruban, Higher plant photosystem II light-harvesting antenna, not the reaction center, determines the excited-state lifetime-both the maximum and the nonphotochemically quenched, Biophys. J. 102 (2012) 2761–2771.
[21] S. Crouchman, A. Ruban, P. Horton, PsbS enhances nonphotochemical fluorescence quenching in the absence of zeaxanthin, FEBS Lett. 580 (2006) 2053–2058.
[22] M.P. Johnson, A. Zia, A.V. Ruban, Elevated ΔpH restores rapidly reversible photoprotective energy dissipation in *Arabidopsis* chloroplasts deficient in lutein and xanthophyll cycle activity, Planta 235 (2012) 193–204.
[23] A.R. Holzwarth, D. Lenk, P. Jahns, On the analysis of non-photochemical chlorophyll fluorescence quenching curves: I. Theoretical considerations, Biochim. Biophys. Acta 1827 (2013) 786–792.
[24] J.J. Snellenburg, L.M. Wlodarczyk, J.P. Dekker, R. van Grondelle, I.H. van Stokkum, A model for the 77K excited state dynamics in *Chlamydomonas reinhardtii* in state 1 and state 2, Biochim. Biophys. Acta Bioenerg. (2016).
[25] I.H.M. van Stokkum, D.S. Larsen, R. van Grondelle, Global and target analysis of time-resolved spectra, Biochim. Biophys. Acta 1657 (2004) 82–104.
[26] E. Belgio, E. Kapitonova, J. Chmeliov, C.D.P. Duffy, P. Ungerer, L. Valkunas, A.V. Ruban, Economic photoprotection in photosystem II that retains a complete light-harvesting system with slow energy traps, Nat. Commun. 5 (2014) 4433.
[27] A.V. Ruban, E. Belgio, The relationship between maximum tolerated light intensity and photoprotective energy dissipation in the photosynthetic antenna: chloroplast gains and losses, Philos. Trans. R. Soc. B Biol. Sci. 369 (2014).
[28] A.V. Ruban, Quantifying the efficiency of photoprotection, Philos. Trans. R. Soc. Lond. B (2017), http://dx.doi.org/10.1098/rstb.2016.0393 (in press).
[29] A.R. Holzwarth, Y. Miloslavina, M. Nilkens, P. Jahns, Identification of two quenching sites active in the regulation of photosynthetic light-harvesting studied by time-resolved fluorescence, Chem. Phys. Lett. 483 (2009) 262–267.
[30] A.Z. Kiss, A.V. Ruban, P. Horton, The PsbS protein controls the organization of the photosystem II antenna in higher plant thylakoid membranes, J. Biol. Chem. 283 (2008) 3972–3978.
[31] X.-P. Li, A.M. Gilmore, S. Caffarri, R. Bassi, T. Golan, D. Kramer, K.K. Niyogi, Regulation of photosynthetic light harvesting involves intrathylakoid lumen pH sensing by the PsbS protein, J. Biol. Chem. 279 (2004) 22866–22874.
[32] D. Lazár, Chlorophyll a fluorescence rise induced by high light illumination of dark-adapted plant tissue studied by means of a model of photosystem II and considering photosystem II heterogeneity, J. Theor. Biol. 220 (2003) 469–503.
[33] X.G. Zhu, Govindjee, N.R. Baker, E. de Sturler, D.R. Ort, S.P. Long, Chlorophyll a fluorescence induction kinetics in leaves predicted from a model describing each discrete step of excitation energy and electron transfer associated with photosystem II, Planta 223 (2005) 114–133.
[34] A. Stirbet, Govindjee, Chlorophyll a fluorescence induction: a personal perspective of the thermal phase, the J-I-P rise, Photosynth. Res. 113 (2012) 15–61.
[35] H.M. Kalaji, V. Goltsev, M. Brestic, K. Bosa, S.I. Allakhverdiev, R.J. Strasser, Govindjee, In Vivo Measurements of Light Emission in Plants, (2014), pp. 69–96.
[36] D. Joly, R. Carpentier, Sigmoidal reduction kinetics of the photosystem II acceptor side in intact photosynthetic materials during fluorescence induction, Photochem. Photobiol. Sci. 8 (2009) 167–173.

Supplementary data to
A four state parametric model for the kinetics of the non-photochemical quenching in Photosystem II

Joris J. Snellenburg[a], Matthew P. Johnson [b], Alexander V. Ruban[c], Rienk van Grondelle[a], Ivo H.M. van Stokkum*[a]

[a] Institute for Lasers, Life and Biophotonics, Faculty of Sciences, VU University Amsterdam, De Boelelaan 1081, 1081 HV, Amsterdam, The Netherlands.

[b] Department of Molecular Biology and Biotechnology, University of Sheffield, UK
[c] School of Biological and Chemical Sciences, Queen Mary University of London, UK

Contents

Components of a parametric model for PAM curves

This section contains a detailed specification of the function required to fit the PAM quenching analysis curves measured from intact chloroplasts. The fitting function takes into account the possible contributions to the observed chlorophyll fluorescence quantum yield from the supercomplexes Photosystem II (PSII) and Photosystem I (PSI) and (disconnected) Light Harvesting Complex II (LHCII). Here the PSII contribution is assumed to be a linear superposition of four possible states, each with a unique quantum yield, related to the state of the PSII RC (open or closed) and the rate of non-photochemical quenching of the PSII supercomplex. Other contributions such as from disconnected Chlorophyll molecules, different chromophores such as phycobilins (relevant for the measured fluorescence in Cyanobacteria [1] or specific experimentally related background contributions are not included in this specification, but can easily be included if needed. Considering the large number of contributions to the fitting function, it is important to keep the specification as concise as possible. A compact way to list the contributions to the fitting function for a particular pigment-protein complex is using the tensor product (also called outer product) of its independent state vectors:

$$\{o,c\} \otimes \{u,q\} = \{\{ou, oq\}, \{cu, cq\}\} \qquad \text{Eq.S1}$$

The product ***cq*** then represents the function that describes the concentration of PSII in the closed, quenched state. For the total contribution J to the PAM signal each concentration function still needs to be multiplied with its quantum yield

Φ_{kl}^{j}, where the additional indices *k* and *l* represent different light–acclimated states; in the case of PSII *k* takes into account whether the state is open or closed and *l* stands for either a quenched or an unquenched species. This can be achieved by taking the result of the tensor product, flattening the 2 dimensional tensor in a column wise manner $\{ou, oq, cu, cq\}$ and then taking the inner product with the respective yield parameters. This operation is abbreviated using a helper function termed outer product function (OPF), with an additional label to indicate which species it describes. For PSII this is written as:

$$\begin{aligned} J^{PSII} &= OPF^{PSII}\left[\{o,c\},\{u,q\}\right] = OPF\left[\left\{\Phi_{ou}^{PSII},\Phi_{oq}^{PSII},\Phi_{cu}^{PSII},\Phi_{cq}^{PSII}\right\},\left\{\{o,c\},\{u,q\}\right\}\right] = \\ & ou\Phi_{ou}^{PSII} + oq\Phi_{oq}^{PSII} + cu\Phi_{cu}^{PSII} + cq\Phi_{cq}^{PSII} \end{aligned} \quad \text{Eq.S2}$$

And for LHCII, which only occurs in quenched or unquenched form, this is written as:

$$\begin{aligned} J^{LHCII} &= OPF^{LHCII}\left[\{u,q\}\right] = OPF\left[\left\{\Phi_{u}^{LHCII},\Phi_{q}^{LHCII}\right\},\left\{\{u,q\}\right\}\right] = \\ & u\Phi_{u}^{LHCII}, q\Phi_{q}^{LHCII} \end{aligned} \quad \text{Eq.S3}$$

In the case of the contribution from PSI the most compact notation is simply the product of concentration and quantum yield:

$$J^{PSI} = c_{PSI}\Phi^{PSI} \quad \text{Eq.S4}$$

Finally it is necessary to account for the stoichiometry between the contributions using fractional parameters, e.g. for PSII, LHCII and PSI respectively $(1 - fr_{LHCII})$, fr_{LHCII} and fr_{PSI}. This is necessary to account for the relative stoichiometry of the proteins themselves, but also to account for the relative difference in absorption at the excitation wavelength used to excite the sample. In this way, when the contribution of PSI and disconnected LHCII can be neglected the fractional constant is just 1. In the case that PSI can be neglected but there is a fair amount of disconnected LHCII then the fraction also sums up to 1.

In the follow paragraphs the exact equations used to construct the fitting function are listed clustered per light regime (dark adapted sample, quenching inducing high light following darkness, recovery in darkness following high light) and given a label so that they can be referenced in subsequent function definitions using the notation BFS["function_label"], where BFS refers to "Basis Function Set". Below the equations are subsequently explained in the order of the light conditions in the experiment described in the main text (see section "Analyzing a full PAM quenching curve" and **Figure 2**)

Darkness (da)

In the region where there is only measuring light and no source of actinic light, the Photosystem II (PSII) reaction centers (RCs) are assumed to be in the open state. If the sample is also dark adapted (has not seen any strong source of actinic light for a long enough period of time) it is also unquenched. Under these light conditions PSII has a fluorescence quantum yield Φ_{ou}^{PSII}. However at the same time it is possible to have contributions to the total signal of unconnected Light Harvesting Complex II (LHCII) and Photosystem I (PSI). This can then be summarized in the equation for a dark adapted ("da") segment:

$$\text{"da"} \rightarrow (1 - fr_{LHCII})\Phi_{ou}^{PSII} + fr_{LHCII}\Phi_{u}^{LHCII} + fr_{PSI}\Phi^{PSI} \quad \text{Eq.S5}$$

The next change in light conditions is a saturation pulse applied at time t_0, with the continuous actinic light source still switched off. To describe the sudden rise in measured fluorescence quantum yield, due to the closing of PSII RC's, a mono exponential function is used "dkspIRF" with rate constant k_1. The subsequent recovery toward the level where all PSII RC's are again open is modeled using three exponential decays (rate constants k_2, k_3, k_{3b}).

$$\text{"dkspIRF"} \rightarrow e^{-k_1^L(t-t_0)}, \text{"dkspD1"} \rightarrow e^{-k_2^L(t-t_0)}, \text{"dkspD2"} \rightarrow e^{-k_3^L(t-t_0)}, \text{"dkspD2b"} \rightarrow e^{-k_{3b}^L(t-t_0)} \quad \text{Eq.S6}$$

Here L represents a label to distinguish the parameters for the same function used in different light conditions. The same functional description can then be used to describe the effect of a specific change in light conditions (e.g. a saturating pulse in darkness) but observed differences in kinetics can then be taken into account by freeing some

parameters. The data described in the main manuscript required freeing the rate k_3 between the first two saturating pulses in darkness for a dark acclimated sample, and the remaining saturating pulses in darkness for a sample that had already been exposed to high light. Then for the first two saturation pulses in darkness k_3 is then defined as k_3^{SP1} and for the rest the parameter k_3^{D1} is used. The rates k_2^{D1}, k_{3b}^{D1} are the same (linked) throughout.

A careful reader might notice that the fluorescence induction dynamics and subsequent relaxation is captured using just a few exponentials, implying underlying first order differential equations. This is a strong assumption but not a necessary one. If more information is available on the dynamics of a particular transition this a priori knowledge can be used to refine the components of the fit function.

With the above definitions the rise of the fluorescence in darkness can be written as:

$$\text{"dkspR"} \rightarrow (1 - fr_{\text{LHCII}})\,\text{OPF}\left[\left\{\begin{matrix}\Phi_{\text{ou}}^{\text{PSII}},\\ \Phi_{\text{cu}}^{\text{PSII}}\end{matrix}\right\}, \left\{\left\{\begin{matrix}\text{BFS}[\text{"dkspIRF"}],\\ 1-\text{BFS}[\text{"dkspIRF"}]\end{matrix}\right\}\right\}\right] + fr_{\text{LHCII}}\Phi_{\text{u}}^{\text{LHCII}} + fr_{\text{PSI}}\Phi^{\text{PSI}} \qquad \text{Eq.S7}$$

The subsequent decay is then described as:

$$\begin{aligned}\text{"dkspD"} \rightarrow (1 - fr_{\text{LHCII}})\,\text{OPF}&\left[\left\{\begin{matrix}\Phi_{\text{ou}}^{\text{PSII}},\\ \Phi_{\text{cu}}^{\text{PSII}}\end{matrix}\right\}, \left\{\left\{\begin{matrix}\left(\begin{matrix}fr_2^{\text{L}}\left(1-\text{BFS}[\text{"dkspD1"}]\right)+\\ \left(1-fr_{3\text{b}}^{\text{L}}\right)\left(1-fr_2^{\text{L}}\right)\left(1-\text{BFS}[\text{"dkspD2"}]\right)+\\ fr_{3\text{b}}^{\text{L}}\left(1-fr_2^{\text{L}}\right)*\left(1-\text{BFS}[\text{"dkspD2b"}]\right)\end{matrix}\right),\\ \left(\begin{matrix}fr_2^{\text{L}}*BFS[\text{"dkspD1"}]+\\ \left(1-fr_{3\text{b}}^{\text{L}}\right)*\left(1-fr_2^{\text{L}}\right)*\text{BFS}[\text{"dkspD2"}]+\\ fr_{3\text{b}}^{\text{L}}*\left(1-fr_2^{\text{L}}\right)*\text{BFS}[\text{"dkspD2b"}]\end{matrix}\right)\end{matrix}\right\}\right]\right]\\ &+ fr_{\text{LHCII}}\Phi_{\text{u}}^{\text{LHCII}} + fr_{\text{PSI}}\Phi^{\text{PSI}}\end{aligned} \qquad \text{Eq.S8}$$

Where the fractional parameters $fr_2^{\text{L}}, fr_{3\text{b}}^{\text{L}}$ are introduced to express the amplitudes of the exponential decays of Eq.S6. For the first two periods of darkness these parameters are defined as $fr_2^{D1}, fr_{3\text{b}}^{D1}$, expect for the first saturating pulse which uses $fr_2^{SP1}, fr_{3\text{b}}^{SP1}$.

Darkness to high light (dk2hl)

When a period of (high) continuous actinic light follows a period of darkness a number of additional function definitions are needed. First the function "dkendC" evaluates the function "dkspD" for the time point just before the dark to light transition t_{LR1end} and quantifies the amount of closed PSII left over due to only partial recovery from a saturating pulse in darkness.

$$\text{"dkendC"} \rightarrow \text{BFS}[\text{"dkspD"}] \text{ with } t \rightarrow t_{LR1end} \qquad \text{Eq.S9}$$

The fluorescence induction dynamics due to the continuous actinic light is again described using a single exponential, but with a different rate constant.

$$\text{"dkhlIRF"} \rightarrow e^{-k_{10}^{L}(t-t_0)} \qquad \text{Eq.S10}$$

Assuming that upon switching to continuous light all the PSII RCs are closed, a small fraction (depending on the absolute level of light intensity) of the RCs can again re-open if the excitation pressure is not enough to keep them completely closed, which is accounted for using a single exponential, where a certain fraction $\left(1 - fr_{\text{CC}}^{\text{H1}}\right)$ of the PSII RCs reopens. The amount of closed PSII can then be described as

$$\text{"hlPSIIc"} \rightarrow \left(1 - fr_{CC}^{H1}\right) e^{-k_6 (t - t_{LLR})} + fr_{CC}^{H1} \qquad \text{Eq.S11}$$

where t_{LLR} is substituted with the timepoint of the last light regime (thus $(t - t_{LLR})$ is the time since switching on the actinic light). The amount of open PSII RCs is simply one minus the closed concentration.

$$\text{"hlPSIIo"} \rightarrow 1 - \text{BFS}[\text{"hlPSIIc"}] \qquad \text{Eq.S12}$$

Using these function definitions the amount of PSII closed/open in the darkness to high light transition can be written as

$$\begin{gathered} \text{"dk2hlPSIIc"} \rightarrow \text{BFS}[\text{"dkendC"}] + \left(1 - \text{BFS}[\text{"dkendC"}]\right) \text{BFS}[\text{"hlPSIIc"}] \left(1 - \text{BFS}[\text{"dkhlIRF"}]\right) \\ \text{"dk2hlPSIIo"} \rightarrow 1 - \text{BFS}[\text{"dk2hlPSIIc"}] \end{gathered} \qquad \text{Eq.S13}$$

During a period of high light non-photochemical quenching is induced, leading to a lower observed fluorescence quantum yield. This is captured in a quenching function which describes the decay of the unquenched population.

To account for a small fraction of initially quenched PSII we define two functions. A fraction fr_{isq} which can be a left over from a previous partial recovery, and a fraction fr_{ifq} due to very fast quenching unresolvable given the limited time-resolution of the experiment (60ms time steps in this case).

$$\text{"ISQ"} \rightarrow fr_{isq}^{L}, \text{"IFQ"} \rightarrow fr_{ifq}^{L} \qquad \text{Eq.S14}$$

Out of the total amount that can be quenched fr_{Q}^{H1} a certain fraction is associated with a relatively slow recovery and therefore indicated with the label "SQ": fr_{SQ}^{H1}, described by a single exponential. Another fraction recovers relatively quickly "FQ": $1 - fr_{SQ}^{H1}$, and can be fitted as the sum of 2 exponentials.

$$\begin{aligned} \text{"hlUnQS"} &\rightarrow \left(1 - \text{BFS}[\text{"ISQ"}]\right) fr_{SQ}\, e^{-k_{4a}^{H1}\left(t - t_{LR\_1}\right)} \\ \text{"hlUnQF"} &\rightarrow \left(1 - \text{BFS}[\text{"IFQ"}]\right)\left(fr_4^{H1}\, e^{-k_4^{H1}\left(t - t_{LR\_1}\right)} + \left(1 - fr_4^{H1}\right) e^{-k_5^{H1}\left(t - t_{LR\_1}\right)} \right) \end{aligned} \qquad \text{Eq.S15}$$

The total function for the relative amount of unquenched and quenched concentration is then written as:

$$\begin{gathered} \text{"hlUnQ"} \rightarrow \left(1 - fr_Q\right) + fr_Q * \left(fr_{SQ}\, \text{BFS}[\text{"hlUnQS"}] + \left(1 - fr_{SQ}\right) \text{BFS}[\text{"hlUnQF"}] \right) \\ \text{"hlQ"} \rightarrow 1 - \text{BFS}[\text{"hlUnQ"}] \end{gathered} \qquad \text{Eq.S16}$$

The full expression to describe the darkness to high light transition can now be assembled:

$$\begin{aligned} \text{"dk2hl"} \rightarrow \left(1 - fr_{LHCII}\right) \text{OPF}^{PSII} \left[\begin{Bmatrix} \left\{ \left(\text{BFS}[\text{"dk2hlPSIIo"}]\right), \text{BFS}[\text{"dk2hlPSIIc"}] \right\}, \\ \left\{ \text{BFS}[\text{"hlQ"}], \text{BFS}[\text{"hlUnQ"}] \right\} \end{Bmatrix} \right] + \\ fr_{LHCII}\, \text{OPF}^{LHCII} \left[\left\{ \left\{ \text{BFS}[\text{"hlQ"}], \text{BFS}[\text{"hlUnQ"}] \right\} \right\} \right] + fr_{PSI} \Phi^{PSI} \end{aligned} \qquad \text{Eq.S17}$$

During the period of continuous actinic light, there are also periodically saturating pulses given to ensure that all PSII RCs are fully closed. The necessary function to fit this aspect in the data is similar to the saturating pulses applied during darkness expect that the kinetics is much faster and both the rise and decay can be fitted with a single exponential.

$$\text{"hlspIRF"} \to e^{-k_1^{H1}(t-t_0)} \text{ , "hlspD1"} \to e^{-k_2^{H1}(t-t_0)} \qquad \text{Eq.S18}$$

This then leads to the amount of open/closed PSII during a saturating pulse during high light being described by:

$$\begin{aligned} \text{"hlspPSIIo"} &\to \text{BFS}[\text{"hlspIRF"}]\left(1-\text{BFS}[\text{"hlPSIIc"}]\right) \\ \text{"hlspPSIIc"} &\to \text{BFS}[\text{"hlPSIIc"}]+\left(1-\text{BFS}[\text{"hlspIRF"}]\right)\left(1-\text{BFS}[\text{"hlPSIIc"}]\right) \end{aligned} \qquad \text{Eq.S19}$$

When the above function definitions are combined the expression for the rise and decay of fluorescence yield during actinic light can respectively be written as:

$$\begin{aligned} \text{"hlspR"} \to \left(1- fr_{\text{LHCII}}\right)\text{OPF}^{\text{PSII}} &\left[\begin{Bmatrix}\{\left(\text{BFS}[\text{"hlspPSIIo"}]\right),\text{BFS}[\text{"hlspPSIIc"}]\},\\ \{\text{BFS}[\text{"hlQ"}],\text{BFS}[\text{"hlUnQ"}]\}\end{Bmatrix}\right]+ \\ fr_{\text{LHCII}}\,\text{OPF}^{\text{LHCII}}&\left[\{\{\text{BFS}[\text{"hlQ"}],\text{BFS}[\text{"hlUnQ"}]\}\}\right]+ fr_{\text{PSI}}\Phi^{\text{PSI}} \end{aligned} \qquad \text{Eq.S20}$$

$$\begin{aligned} \text{"hlspD"}->\left(1- fr_{\text{LHCII}}\right)\text{OPF}^{\text{PSII}} &\left[\begin{Bmatrix}\{\left(\left(1-\text{BFS}[\text{"hlspD1"}]\right)\text{BFS}[\text{"hlPSIIo"}]\right),\\ \left(1-\text{BFS}[\text{"hlPSIIc"}]\right)\text{BFS}[\text{"hlspD1"}]+\text{BFS}[\text{"hlPSIIc"}]\}\\ \{\text{BFS}[\text{"hlQ"}],\text{BFS}[\text{"hlUnQ"}]\}\end{Bmatrix},\right]+ \\ fr_{\text{LHCII}}\,\text{OPF}^{\text{LHCII}}&\left[\{\{\text{BFS}[\text{"hlQ"}],\text{BFS}[\text{"hlUnQ"}]\}\}\right]+ fr_{\text{PSI}}\Phi^{\text{PSI}} \end{aligned} \qquad \text{Eq.S21}$$

High light to darkness or recovery (hl2dk)

In a period of darkness, following actinic light, the induced non-photochemical quenching gradually recovers. The starting point for the recovery can be determined by evaluating the quenching function at the end of the high light period, just before the recovery period.

$$\begin{aligned} \text{"SQT"} &\to \left(1-\text{BFS}[\text{"hlUnQS"}]\right)\text{with } t-t_{\text{LR\_1}} \to t_{\text{LR\_1}}-t_{\text{LR\_2}} \\ \text{"FQT"} &\to \left(1-\text{BFS}[\text{"hlUnQF"}]\right)\text{with } t-t_{\text{LR\_1}} \to t_{\text{LR\_1}}-t_{\text{LR\_2}} \end{aligned} \qquad \text{Eq.S22}$$

The dynamics of recovery consists of two parts both fitted with a single exponential. One part of the induced quenching is recovered from very slowly ($fr_{\text{SQ}}^{\text{H1}}$) given by rate k_{8a}, while the other part recovers quickly $\left(1- fr_{\text{SQ}}^{\text{H1}}\right)$ given by rate k_8.

$$\begin{aligned} \text{"hldkRecF"} &\to \left(1-e^{-k_8^{\text{R1}}\left(t-t_{\text{LR\_1}}\right)}\right)\text{ , "hldkRecS"} \to \left(1-e^{-k_{8a}^{\text{R1}}\left(t-t_{\text{LR\_1}}\right)}\right), \\ \text{"hldkRec"} &\to fr_{\text{Q}}^{\text{H1}}\left(fr_{\text{SQ}}^{\text{H1}}\,\text{BFS}[\text{"hldkRecS"}])+\left(1- fr_{\text{SQ}}^{\text{H1}}\right)\text{BFS}[\text{"hldkRecF"}]\right), \end{aligned} \qquad \text{Eq.S23}$$

While recovery from NPQ is a relatively slow process, the reopening of PSII RCs is quite fast and results in a quick transition from mostly closed PSII RCs in actinic light, to completely open RCs in the recovery phase. The dynamics of this transition is captured by the same function which describes reopening after a saturating pulse.

$$\begin{aligned} \text{"hl2dkPSIIo"} \to\ & fr_2^{\text{L}}\left(1-\text{BFS}[\text{"dkspD1"}]\right)+\left(1- fr_{3\text{b}}^{\text{L}}\right)\left(1- fr_2^{\text{L}}\right)\left(1-\text{BFS}[\text{"dkspD2"}]\right)+ \\ & fr_{3\text{b}}^{\text{L}}\left(1- fr_2^{\text{L}}\right)*\left(1-\text{BFS}[\text{"dkspD2b"}]\right) \\ \text{"hl2dkPSIIc"} \to\ & fr_2^{\text{L}}\,BFS\left[\text{"dkspD1"}\right]+\left(1- fr_{3\text{b}}^{\text{L}}\right)\left(1- fr_2^{\text{L}}\right)\text{BFS}[\text{"dkspD2"}]+ \\ & fr_{3\text{b}}^{\text{L}}\left(1- fr_2^{\text{L}}\right)*\left(\text{BFS}[\text{"dkspD2b"}]\right) \end{aligned} \qquad \text{Eq.S24}$$

With fr_2^{L}, $fr_{3\text{b}}^{\text{L}}$ equal to fr_2^{D1}, $fr_{3\text{b}}^{\text{D1}}$ during the first recovery period and fr_2^{R2}, $fr_{3\text{b}}^{\text{R2}}$ during the second recovery period.

Finally the amount of unquenched and quenched PSII can then be expressed as:

$$
\begin{aligned}
\text{"hl2dkPSIIuS"} &\to \left(\left(1-\text{BFS}\left[\text{"SQT"}\right]\right)+\text{BFS}\left[\text{"SQT"}\right]\text{BFS}\left[\text{"hldkRecS"}\right]\right),\\
\text{"hl2dkPSIIuF"} &\to \left(\left(1-\text{BFS}\left[\text{"FQT"}\right]\right)+\text{BFS}\left[\text{"FQT"}\right]\text{BFS}\left[\text{"hldkRecF"}\right]\right),\\
\text{"hl2dkPSIIu"} &\to fr_{\text{Q}}\left(\left(1-fr_{\text{SQ}}\right)\text{BFS}\left[\text{"hl2dkPSIIuF"}\right]+fr_{\text{SQ}}\,\text{BFS}\left[\text{"hl2dkPSIIuS"}\right]\right),\\
\text{"hl2dkPSIIq"} &\to 1-\text{BFS}\left[\text{"hl2dkPSIIu"}\right],
\end{aligned}
\qquad \text{Eq.S25}
$$

The function definition that describes the quenching of LHCII can be postulated in the same way, but is not specified here in detail as there is no data in the main text to test it against. In a first approximation the quenching dynamics can be assumed to be the same as for the LHCII-PSII complex. When these functions are combined the function that described the transition from darkness to high light can be written as:

$$
\begin{aligned}
\text{"dk2hl"} \to{}& \left(1-fr_{\text{LHCII}}\right)\text{OPF}^{\text{PSII}}\left[\begin{Bmatrix}\left\{\left(\text{BFS}\left[\text{"hl2dkPSIIo"}\right]\right),\text{BFS}\left[\text{"hl2dkPSIIc"}\right]\right\},\\ \left\{\text{BFS}\left[\text{"hl2dkPSIIq"}\right],\text{BFS}\left[\text{"hl2dkPSIIu"}\right]\right\}\end{Bmatrix}\right]+\\
& fr_{\text{LHCII}}\,\text{OPF}^{\text{LHCII}}\left[\left\{\left\{\text{BFS}\left[\text{"hl2dkLHCIIq"}\right],\text{BFS}\left[\text{"hl2dkLHCIIu"}\right]\right\}\right\}\right]+fr_{\text{PSI}}\Phi^{\text{PSI}}
\end{aligned}
\qquad \text{Eq.S26}
$$

The rise of fluorescence due to a saturating pulse in darkness, taking into account the baseline level of recovery can be written as:

$$
\begin{aligned}
\text{"recPSIIc"} &\to \left(1-\text{BFS}\left[\text{"hl2dkPSIIc"}\right]\right)\left(1-\text{BFS}\left[\text{"dkspIRF"}\right]\right)+\text{BFS}\left[\text{"hl2dkPSIIc"}\right]\\
\text{"recPSIIo"} &\to 1-\text{BFS}\left[\text{"recPSIIc"}\right]
\end{aligned}
\qquad \text{Eq.S27}
$$

Finally making use of the above function definitions, the function that describe the segments in the recovery regime during and between saturating pulses can be formulated as:

$$
\begin{aligned}
\text{"recspR"} \to{}& \left(1-fr_{\text{LHCII}}\right)\text{OPF}^{\text{PSII}}\left[\begin{Bmatrix}\left\{\text{BFS}\left[\text{"recPSIIo"}\right],\text{BFS}\left[\text{"recPSIIc"}\right]\right\},\\ \left\{\text{BFS}\left[\text{"hl2dkPSIIq"}\right],\text{BFS}\left[\text{"hl2dkPSIIu"}\right]\right\}\end{Bmatrix}\right]+\\
& fr_{\text{LHCII}}\,\text{OPF}^{\text{LHCII}}\left[\left\{\left\{\text{BFS}\left[\text{"hl2dkLHCIIq"}\right],\text{BFS}\left[\text{"hl2dkLHCIIu"}\right]\right\}\right\}\right]+fr_{\text{PSI}}\Phi^{\text{PSI}}\\
\text{"recspD"} \to{}& \left(1-fr_{\text{LHCII}}\right)\text{OPF}^{\text{PSII}}\left[\begin{Bmatrix}\left\{\left\{\left(\text{BFS}\left[\text{"hl2dkPSIIo"}\right]\right),\left(\text{BFS}\left[\text{"hl2dkPSIIc"}\right]\right)\right\},\\ \left\{\text{BFS}\left[\text{"hl2dkPSIIq"}\right],\text{BFS}\left[\text{"hl2dkPSIIu"}\right]\right\}\end{Bmatrix}\right]+\\
& fr_{\text{LHCII}}\,\text{OPF}^{\text{LHCII}}\left[\left\{\left\{\text{BFS}\left[\text{"hl2dkLHCIIq"}\right],\text{BFS}\left[\text{"hl2dkLHCIIu"}\right]\right\}\right\}\right]+fr_{\text{PSI}}\Phi^{\text{PSI}}
\end{aligned}
\qquad \text{Eq.S28}
$$

Together these labeled functions can be used to model all the different changes in light conditions that are observed in the data reported in the main text.

Working model for the sample devoid of zeaxanthin

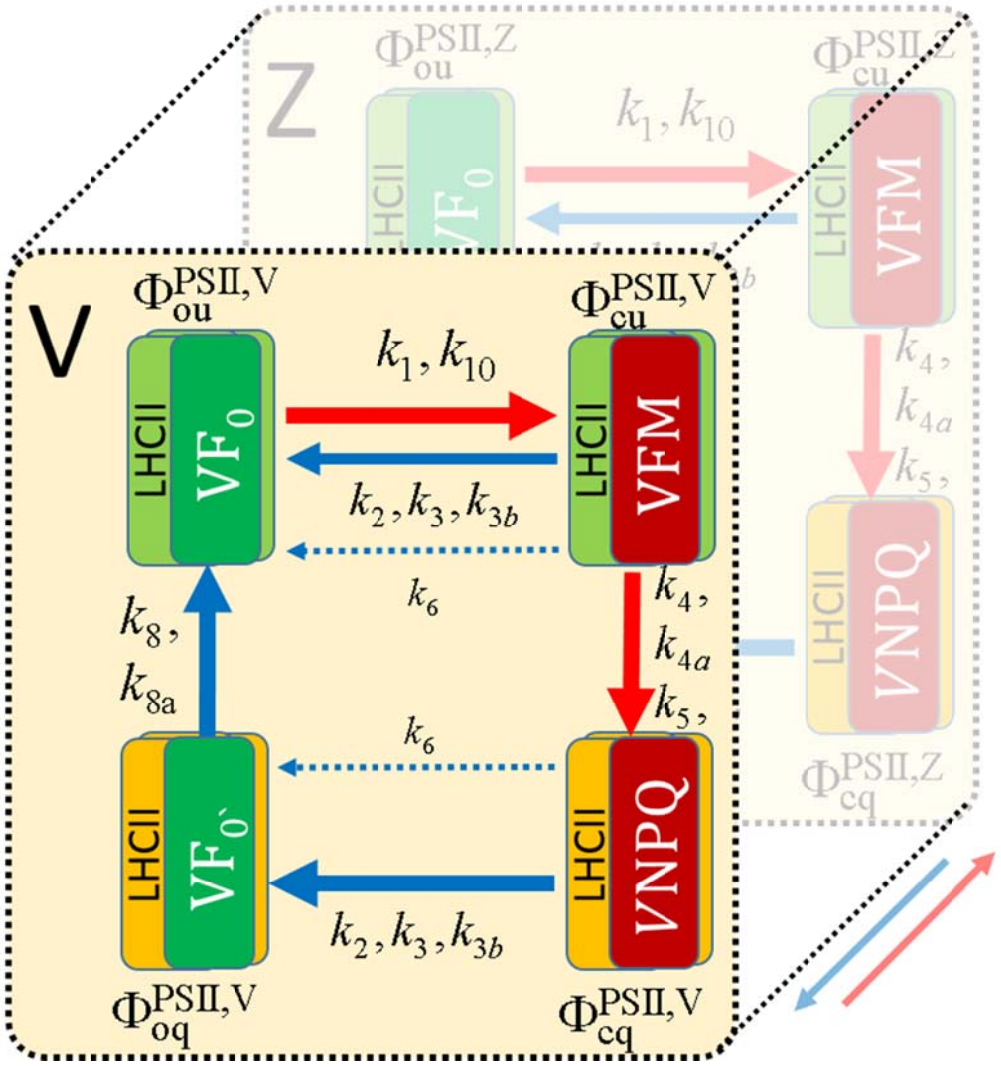

Figure S 1. Working mathematical model which ties the different species listed in Figure 1 to the parametric description given in equation (2) for the sample devoid of zeaxanthin (V). The premise of the model are four distinct states which can be interconverted into one another with certain rates, either light driven (red arrows) or spontaneously in the absence of light (blue arrows). The difference with the model for the Z case is an additional rate k_6 which represents re-opening of the reaction centers due to insufficient actinic light pressure to keep them completely closed. A simplification of the model is the assumption that the sample remains devoid of zeaxanthin over the course of the measurement.

Segments	Label	Description	Parameters introduced
1,2[1]	"bg"	Background signal, measuring light (ML) OFF	
3	"da"	Signal from a dark adapted sample (ML ON)	Φ_{ou}^{PSII}; $fr_{LHCII}, \Phi_{u}^{LHCII}$; fr_{PSI}, Φ^{PSI}
4,6	"dkspR"	Saturating pulse *rise* in darkness	Φ_{cu}^{PSII}, k_1^{D1}
5,7,8[1]	"dkspD"	Saturating pulse *decay* in darkness	$k_2^{D1}, k_3^{D1}, k_{3b}^{D1}, fr_2^{D1}, fr_{3b}^{D1}$, optionally $fr_2^{SP1}, fr_{3b}^{SP1}, k_3^{SP1}$
9	"dk2hl" (1)	Darkness to (high) actinic light	$\Phi_{oq}^{PSII}, \Phi_{cq}^{PSII}, fr_Q^{H1}, fr_{SQ}^{H1}, fr_4^{H1}, k_4^{H1}, k_5^{H1}, k_{10}^{D1}, fr_{CC}^{H1}, k_6^{H1}; \Phi_q^{LHCII}$
10,12,…,22	"hlspR" (1)	Saturating pulse *rise* in actinic light	k_1^{H1}
11,13,…,23	"hlspD" (1)	Saturating pulse *decay* in actinic light	k_2^{H1}
24[1],25	"hl2dk" (1)	Actinic light to darkness transition	k_8^{R1}, k_{8a}^{R1}, optionally fr_2^{R1}, fr_{3b}^{R1}
26,28,…,38	"recspR" (1)	Saturating pulse *rise* in darkness during recovery	
27,29,…39,40[1]	"recspD" (1)	Saturating pulse *decay* in darkness during recovery	
41	"dk2hl" (2)	Darkness to (high) actinic light (after recovery)	optionally $fr_4^{H2}, k_4^{H2}, k_5^{H2}$ and k_6^{H2}
42,44,…58	"hlspR" (2)	Saturating pulse *rise* in actinic light (after recovery)	
43,45,…59	"hlspD" (2)	Saturating pulse *decay* in actinic light (after recovery)	
60[1],61	"hl2dk" (2)	2nd Actinic light to darkness transition	optionally fr_2^{R2}, fr_{3b}^{R2}
62,64,…,74	"recspR" (2)	Saturating pulse *rise* in darkness during 2nd recovery	
63,65,…,75,76[1]	"recspD" (2)	Saturating pulse *decay* in darkness during 2nd recovery	
77	"bg"	Background signal after turning ML OFF.	

Table S 1: Full parameter table for the total fitting function for the 77 segments of the data. For each label a closed form expression is available in the present section. Labels (1) and (2) signify the first and second time a particular expression is used, for which the estimated parameters can have different numerical values. All parameters introduced for a function in a particular segment can be optionally made free in repeated occurrences of that function for subsequent segments. Specifically some parameters are listed here explicitly because they were freed in fitting one of the datasets described in the main text.

For SP1 $a_2 = fr_2^{SP1}, a_3 = \left(1-fr_{3b}^{SP1}\right)\left(1-fr_2^{SP1}\right), a_{3b} = fr_{3b}^{SP1}\left(1-fr_2^{SP1}\right)$

For SP2 $a_2 = fr_2^{D1}, a_3 = \left(1-fr_{3b}^{D1}\right)\left(1-fr_2^{D1}\right), a_{3b} = fr_{3b}^{D1}\left(1-fr_2^{D1}\right)$

Table S 2. Relation between amplitude parameters used in the main text and fractions given in **Table S 1**.

[1] These segments consist of only a single data point, between the end of one light regime and the start of the next. To describe this one transition point, the function of the previous or the next light regime is reused. This is a mechanism to deal with non-instantaneous light switching, although for the data reported in this simulation the switching occurred within the 60 ms time steps of the data.

```
In[222]:= Clear[xFrom, xTo, step];
          With[
           {args = Delete[parameterListZ, 0],
            controls = Join[parameterSettingsZ, {"Manipulate settings:", {{xFrom, 1}, 1, Length[r_timesZ] - 1}, {{xTo, Length[r_timesZ]}, 2, Length[r_timesZ]}, {{step, 1}, {1, 2, 5, 10, 50, 100, 200}}}]},
           Manipulate[
            lowWeightFrom = 100;
          simdataZ = SimPamFZ[#, args] & /@ r_timesZ;
            plotdataZ = Transpose[{r_timesZ, simdataZ}];
            resdataZ = r_rawdataZ - simdataZ;
            resplotdataZ = Transpose[{r_timesZ, resdataZ}];
            ListPlot[{Transpose[{r_timesZ, r_rawdataZ}][[Floor[xFrom] ;; Floor[xTo]]], plotdataZ[[Floor[xFrom] ;; Floor[xTo]]], resplotdataZ[[Floor[xFrom] ;; Floor[xTo]]]},
             PlotRange → {All, {-0.1, 0.7}}, ImageSize → {580, 520}, PlotMarkers → Graphics@{Disk[{0, 0}, Scaled@0.003]}, Joined → {False, True, False}, PlotStyle → {{Orange}, {Red, Thick}, Gray},
             PlotTheme → "Detailed", FrameLabel → {"Time (s)", "Rel. ChlF Yield. (a.u.)"}, BaseStyle → {FontSize → 18}, Frame → {True, True, True, True},
             PlotStyle → Directive[Thick, Black, PointSize[Large]]], Evaluate[Grid[Transpose[Map[Control, Partition[controls, 17], {-3}]]], ControlPlacement → Right, ContentSize → {640, 550}]]
```

Out[223]=

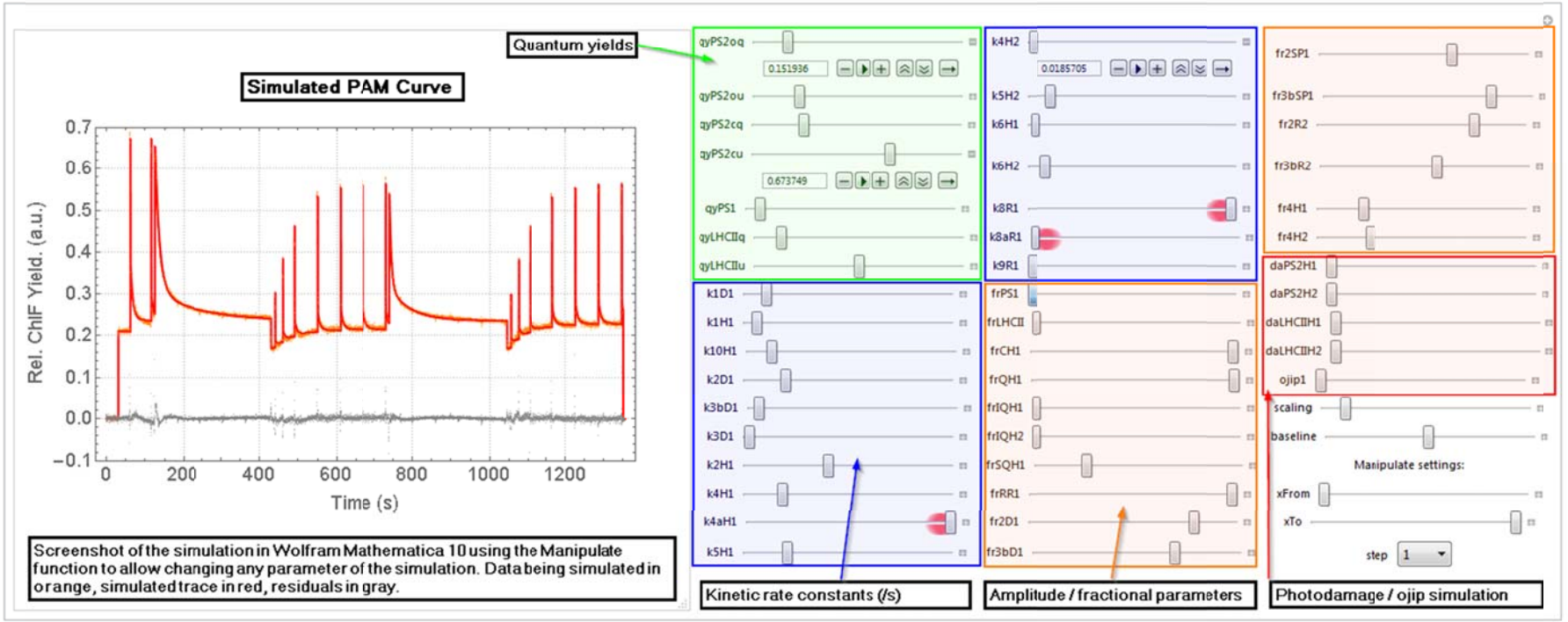

Figure S 2: Annotated screenshot of the simulation of the Z data in Wolfram Mathematica 10. The simulation function is underlined in red and takes as arguments: element out of a list of timepoints (r_timesZ) and arguments for which the controls are shown to the right of the graphics. Note that the variables named differ slightly from those in the main text (most notably k4aH1 = $k_{4a}^{H1} = k_{SQ}^{H1}$), and not all variables are directly relevant for the simulation shown (for instance none of the parameters related to simulating photodamage or different OJIP dynamics are used).

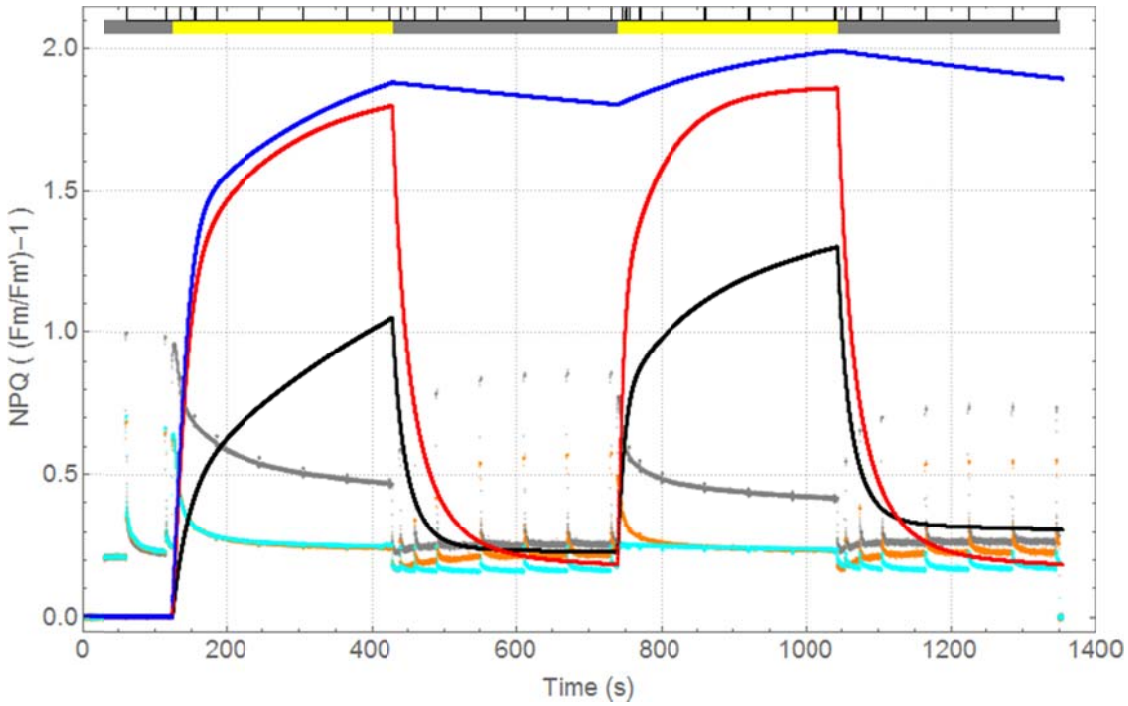

Figure S 3. Level of NPQ (defined as: Fm/Fm' -1) during a fluorescence quenching analysis experiment on intact Chloroplasts devoid of zeaxanthin (black, labeled 'V') or enriched in zeaxanthin (red ('Z'), blue ('GA')). The blue curve represents a sample where glutaraldehyde (GA) was added (at t≈410s) to prevent the recovery from the quenched state. The level of NPQ is calculated directly from the fitting function with the kinetic parameters that describe the decay following a saturating pulse set to zero (i.e. continuously in Fm'). In the background the original data from **Figure 2** of the main text is shown: the V dataset in gray, the Z dataset in orange and the GA dataset in cyan. Light conditions indicated by the top bar as described in the caption of that figure.

The NPQ parameter is a commonly used derived quantity. It is expressed as (Fm/Fm'-1), where Fm is the maximal fluorescence during a saturating pulse in darkness, or alternatively the maximum reached directly after switching on actinic light after a period of dark adaptation, and Fm' the maximal fluorescence reached in a saturating pulse during actinic light exposure. In the context of the functions listed in **Table S 1** and defined above, Fm can be defined as the maximum of the functions labeled "dkspR" or "dk2hl", and Fm' can be defined as the "hlspD" function evaluated with all decay rates set to zero (so that the level stays at the maximum of the "hlspR" function). In the recovery period instead of "hlspD" the function "recspD" is used. In **Figure S 3** the NPQ curves for all datasets are visualized.

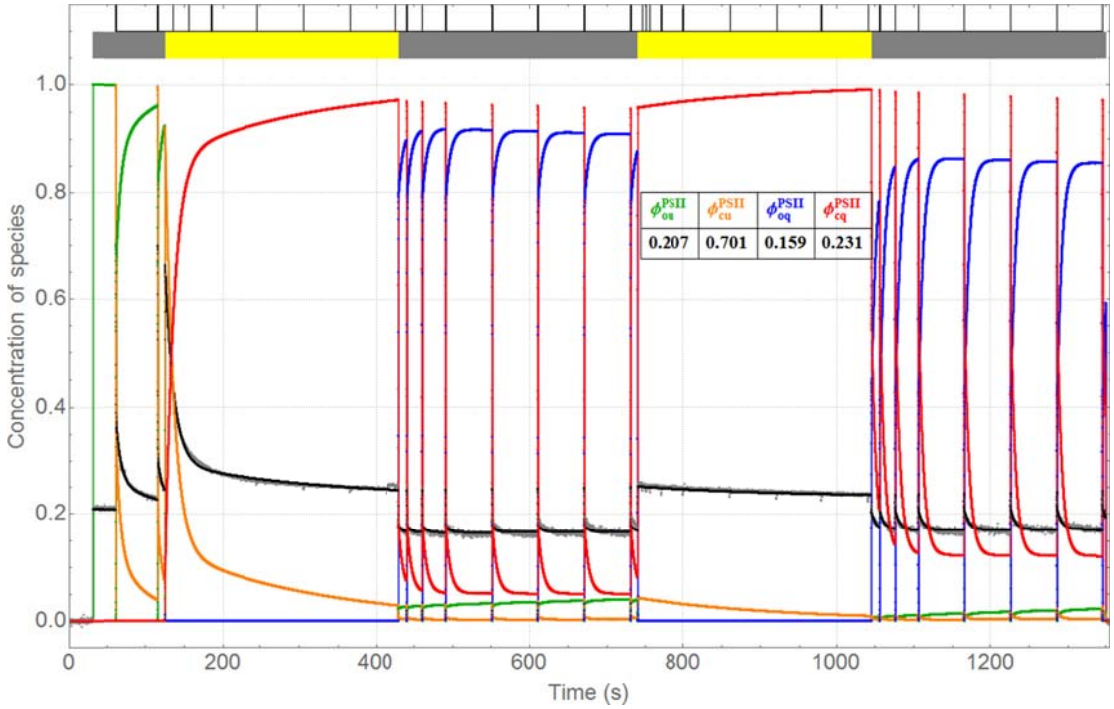

Figure S 4: Concentration profiles of the different states of PSII contributing to the total relative chlorophyll fluorescence quantum yield for the GA dataset. The sum of the concentrations, open unquenched PSII (green, $\Phi_{ou}^{PSII} = 0.207$), closed unquenched PSII (orange, $\Phi_{cu}^{PSII} = 0.701$), open quenched PSII (blue, $\Phi_{cq}^{PSII} = 0.159$) and closed quenched PSII (red, $\Phi_{cq}^{PSII} = 0.231$) multiplied by their respective quantum yields produce the PAM curve depicted in solid black. For comparison the GA observations are overlaid as gray dots. Light conditions indicated by the top bar as described in the caption of **Figure 2**.

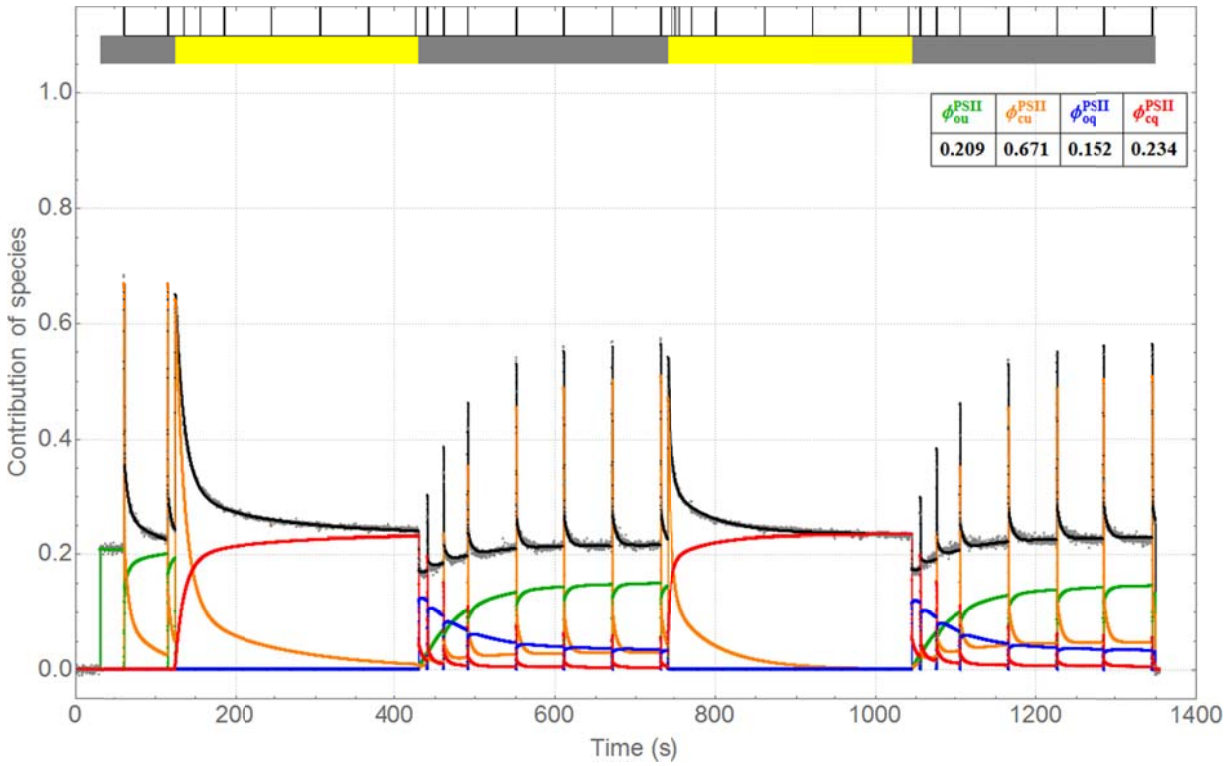

Figure S 5. Contributions of the different states of PSII to the total relative chlorophyll fluorescence quantum yield for the Z dataset. The contribution of a PSII state is defined as the product of its concentrations (shown in **Figure 7**) and the relative quantum yields: open unquenched PSII (green, $\Phi_{ou}^{PSII} = 0.209$), closed unquenched PSII (orange, $\Phi_{cu}^{PSII} = 0.671$), open quenched PSII (blue, $\Phi_{oq}^{PSII} = 0.152$) and closed quenched PSII (red, $\Phi_{cq}^{PSII} = 0.234$). The total fitted contribution is in solid black, observations depicted as gray dots. Light conditions indicated by the top bar as described in the caption of **Figure 2**.

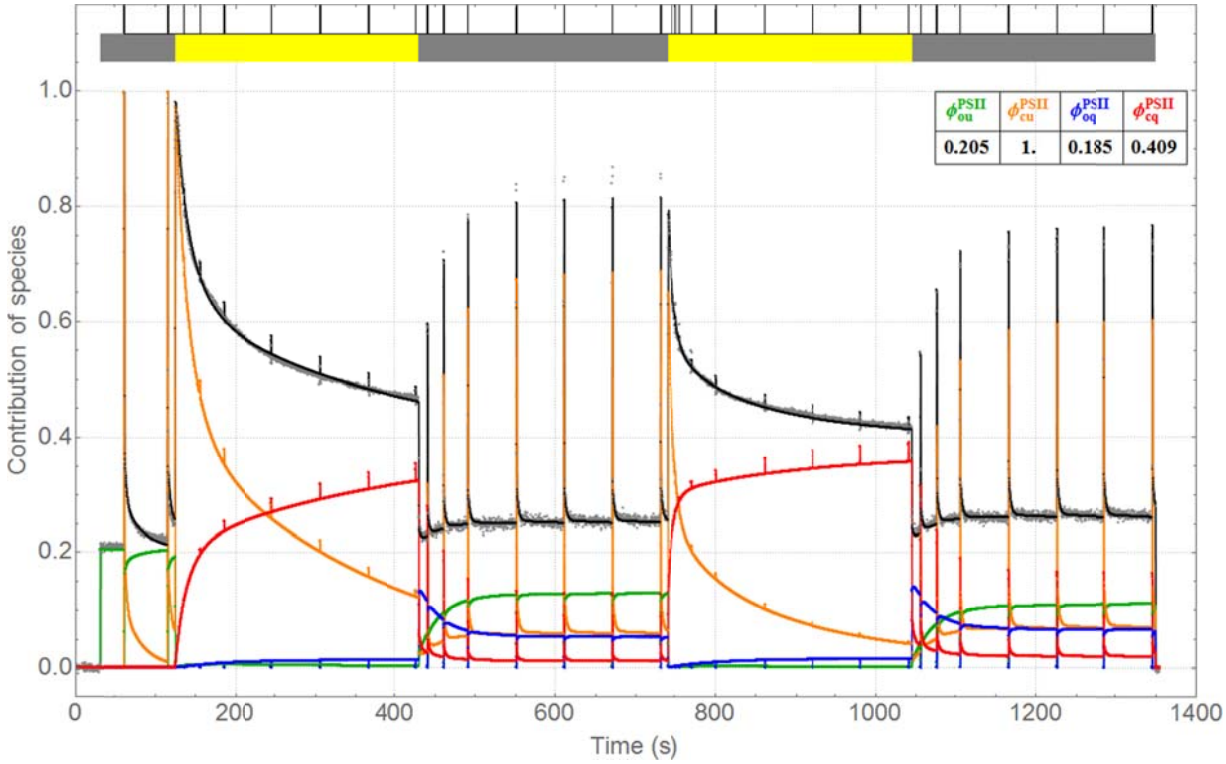

Figure S 6 Contributions of the different states of PSII to the total relative chlorophyll fluorescence quantum yield for the V dataset. The contribution of a PSII state is defined as the product of its concentrations (shown in **Figure 8**) and the relative quantum yields: open unquenched PSII (green, $\Phi_{ou}^{PSII} = 0.205$), closed unquenched PSII (orange, $\Phi_{cu}^{PSII} = 1$), open quenched PSII (blue, $\Phi_{oq}^{PSII} = 0.185$) and closed quenched PSII (red, $\Phi_{cq}^{PSII} = 0.409$). The total fitted contribution is in solid black, observations depicted as gray dots. Light conditions indicated by the top bar as described in the caption of **Figure 2**.

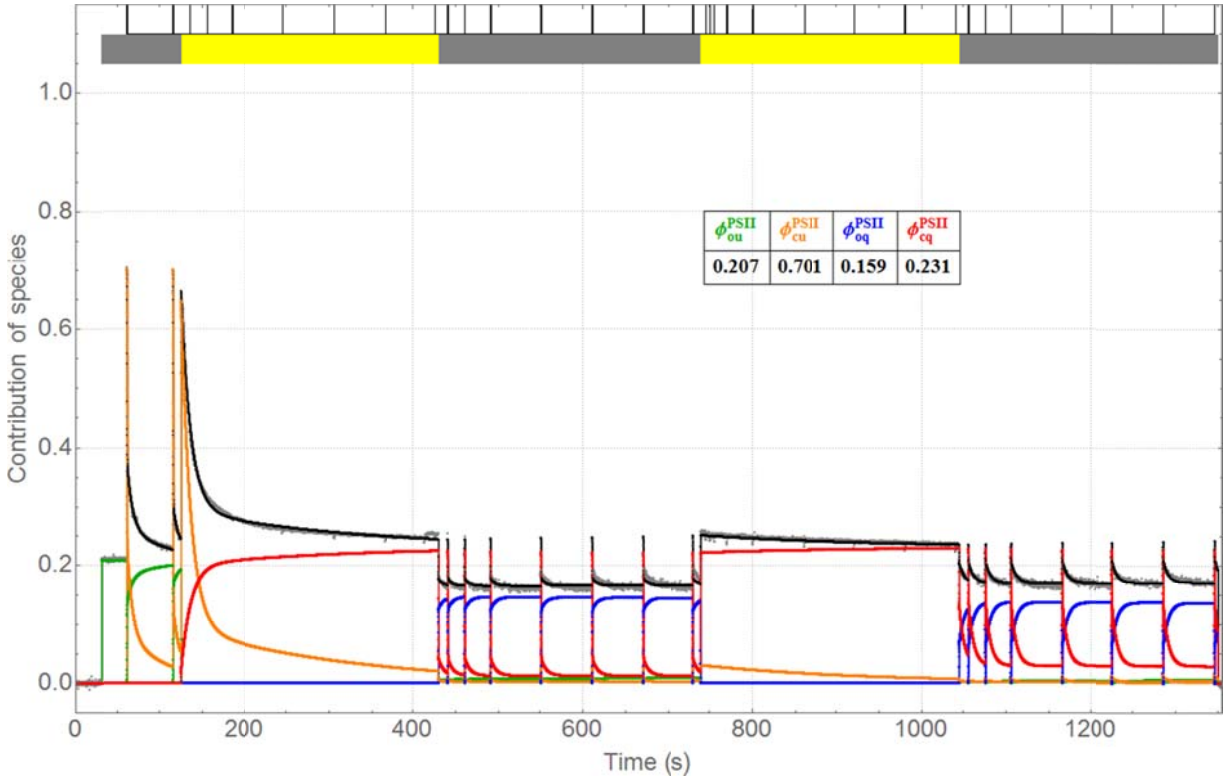

Figure S 7 Contributions of the different states of PSII to the total relative chlorophyll fluorescence quantum yield for the GA dataset. The contribution of a PSII state is defined as the product of its concentrations (shown in Figure S 4) and the relative quantum yields: open unquenched PSII (green, $\Phi_{ou}^{PSII} = 0.207$), closed unquenched PSII (orange, $\Phi_{cu}^{PSII} = 0.701$), open quenched PSII (blue, $\Phi_{oq}^{PSII} = 0.159$) and closed quenched PSII (red, $\Phi_{cq}^{PSII} = 0.231$). The total fitted contribution is in solid black, observations depicted as gray dots. Light conditions indicated by the top bar as described in the caption of **Figure 2**.

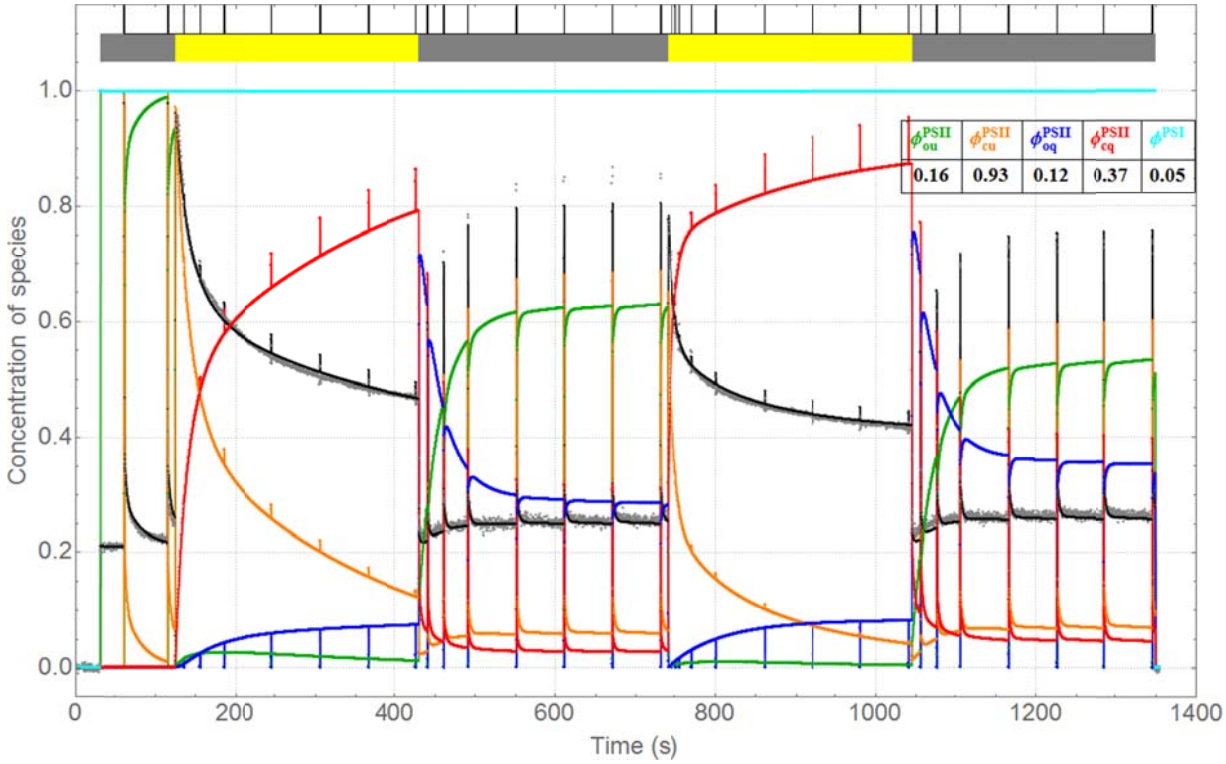

Figure S 8. Concentration profiles of the different states of PSII **and PSI** contributing to the total relative chlorophyll fluorescence quantum yield for the V dataset. The sum of the concentrations, open unquenched PSII (green, $\Phi_{ou}^{PSII} = 0.16$), closed unquenched PSII (orange, $\Phi_{cu}^{PSII} = 0.93$), open quenched PSII (blue, $\Phi_{oq}^{PSII} = 0.12$), closed quenched PSII (red, $\Phi_{cq}^{PSII} = 0.37$) and PSI (cyan, $\Phi^{PSI} = 0.05$) multiplied by their respective quantum yields produce the PAM curve depicted in solid black. For comparison the V observations are overlaid as gray dots. Light conditions indicated by the top bar as described in the caption of **Figure 2**.

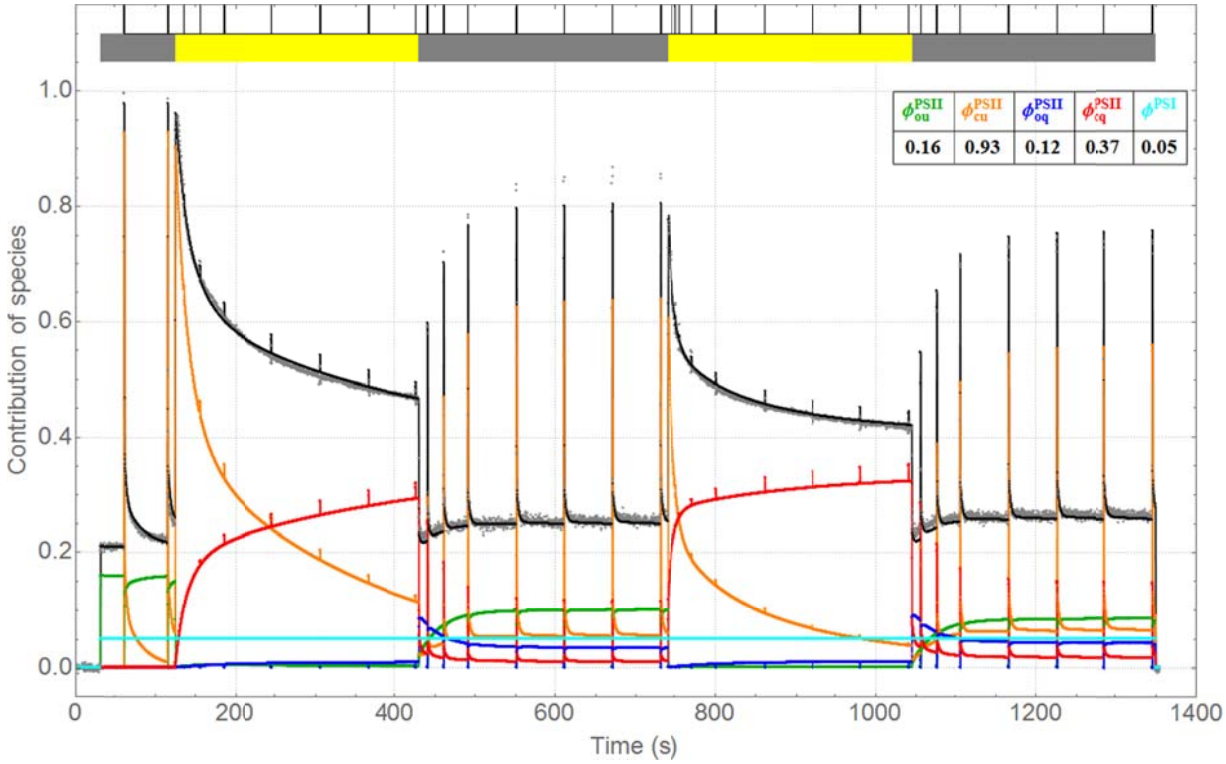

Figure S 9. Contributions of the different states of PSII and PSI to the total relative chlorophyll fluorescence quantum yield for the V dataset. The contribution of a PSII state is defined as the product of its concentrations (shown in Figure S 8) and the relative quantum yields: open unquenched PSII (green, $\Phi_{ou}^{PSII} = 0.16$), closed unquenched PSII (orange, $\Phi_{cu}^{PSII} = 0.93$), open quenched PSII (blue, $\Phi_{oq}^{PSII} = 0.12$), closed quenched PSII (red, $\Phi_{cq}^{PSII} = 0.37$) and PSI (cyan, $\Phi^{PSI} = 0.05$). The total fitted contribution is in solid black, observations depicted as gray dots. Light conditions indicated by the top bar as described in the caption of **Figure 2**.

The link with time-resolved fluorescence spectroscopy

The link with ultrafast time-resolved fluorescence spectroscopy will be established by demonstrating how a target model applied to time-resolved measurements can provide independent estimates of the quantum yields, which can then be compared to those estimated from the quantitative model for PAM fluorometry.
In contrast, ultra-fast time-resolved fluorescence spectroscopy data carries a wealth of information on the picosecond to nanosecond timescales and provides detailed information on the spectral-temporal excited state dynamics upon photo-excitation. However, the experiments are relatively more difficult, take more time and the equipment is costly and cannot easily be carried into the field. Also, putting the system in a particular physiologically relevant condition (quenched, unquenched, closed or open reaction centers (RCs)) and keeping it there for the duration of the measurement is experimentally challenging.
Ultimately however, PAM fluorometry and ultrafast time-resolved fluorescence spectroscopy can be used to probe the same system and both record information on the fluorescence yield, so it should be possible to relate the two experimental techniques to arrive at a more quantitative interpretation of PAM fluorometry curves and potentially bring physiologically relevant parameters to aid in modelling the ultrafast time-resolved fluorescence data using target analysis [2].

Crucial to the decomposition method is the assumption that the measured yield is a superposition of contributions from several species each with their own distinct quantum yield. In intact chloroplasts of plants the general assumption is that the measured yield is due to changes in the efficiency of the photochemistry of PSII, and in line with this assumption so far we have neglected the contribution of PSI. Sometimes the contributions from PSI or disconnected and/or aggregated LHCII antenna need to be taken into account, e.g. in measurements on plants treated with lincomycin which dramatically increases the ratio of antenna per reaction center [3]. For an accurate and quantitative description of the PAM curve good estimates for the relevant quantum yields are necessary, insofar as they cannot be directly estimated from the measured data. In principle the quantum yield can be most accurately estimated from a target analysis of time-resolved spectroscopy data but this requires careful ultra-fast time-resolved measurements in the same conditions as with the PAM measurement. For the V and the Z samples shown in **Figure 2** time-resolved fluorescence data obtained using time-correlated single photon counting (TCSPC) were available [4] which have been re-analyzed using target analysis. Specifically measurements on two states for each of the two samples for a total of four datasets were included in a simultaneous target analysis: closed unquenched ('Fm') and closed quenched ('NPQ') for the sample devoid of Zeaxanthin (VFm, VNPQ) and for the sample enriched in Zeaxanthin (ZFm, ZNPQ) (see also Figure 1). The state of the PSII RCs in the four datasets is assumed to be completely closed for all datasets and either unquenched or fully quenched. Excitation occurred at 470 nm, predominantly exciting Chl b and Carotenoid, and thus relatively more PSII than PSI.

The datasets were first globally analyzed individually, i.e. each dataset represented by a matrix $\Psi(t,\lambda)$ was fitted to the minimal number n_{comp} of exponential decays convolved with an instrument response function (IRF) required to satisfactorily fit the data up to the noise ξ. For each wavelength the amplitude parameters of all exponential decays are determined using the method of variable projection [5] as implemented by the free software TIMP [6] and Glotaran [7]. This results in a decay associated spectrum (DAS) for each component. This can be summarized as:

$$\Psi(t,\lambda) = \sum_{l}^{n_{comp}} \left[\left(\exp[-k_l t] \otimes \mathrm{IRF}(t) \right) \mathrm{DAS}_l(\lambda) \right] + \xi(t,\lambda) \qquad \text{Eq.S29}$$

where k_l is the rate of decay of each component, the reciprocal of which represents the lifetime corresponding to that decay. For each measurement the IRF was independently measured by scattered laser light. Each IRF was characterized by means of a primary Gaussian shaped band, and a number of extra Gaussians shaped bands related to the primary band by a certain scaling factor, a shift in time and a different width. In this way the non-Gaussian nature of the IRF of the TCSPC detector could be very well approximated while maintaining the advantages that a purely analytical model function provides [2] in contrast to numerically convolving the measured IRF with the exponential decays. When fitting the data, all instrument response parameters were fixed except for the position of

the primary Gaussian band which was a free parameter of the fit. This is almost always necessary because the IRF is typically measured at a different wavelength than where the data is measured so there might be a small shift due to dispersion and experimental variation might induce an additional shift. The estimated lifetimes and their Decay Associated Spectra (DAS) are depicted in Figure S 10.

Six components were needed to describe each dataset up to the noise level. The fastest lifetime is shorter than can reliably be estimated given the IRF width (≈110 ps FWHM) but is necessary to account for a bit of relaxation from slightly more blue to redder Chl's in the first tens of ps of the experiment due to a selective excitation of Chl b. The first lifetime that can reliably be resolved is around 0.07-0.1 ns and has a broad emission band peaking around 710 nm, which can safely be attributed to PSI emission. In the ZNPQ datasets this component is likely capturing a small fraction of fast quenching. The next three lifetimes all feature a very similar spectral shape with emission around 680 nm reflecting emission from the LHCII-PSII supercomplex. Clearly quenching is playing a major role on these timescales, differently affecting the samples. The last lifetime represents a tiny fraction of very long lived emission which is observed as a result of measuring for 50 ns. This component likely represents some recombination fluorescence which can safely be ignored. On the basis of one fast component emitting around 710 nm (black DAS) and three DAS with similar shapes (red, blue and magenta) emitting around 680 nm a target model can be constructed consisting of a PSI compartment in parallel to a LHCII-PSII contribution.

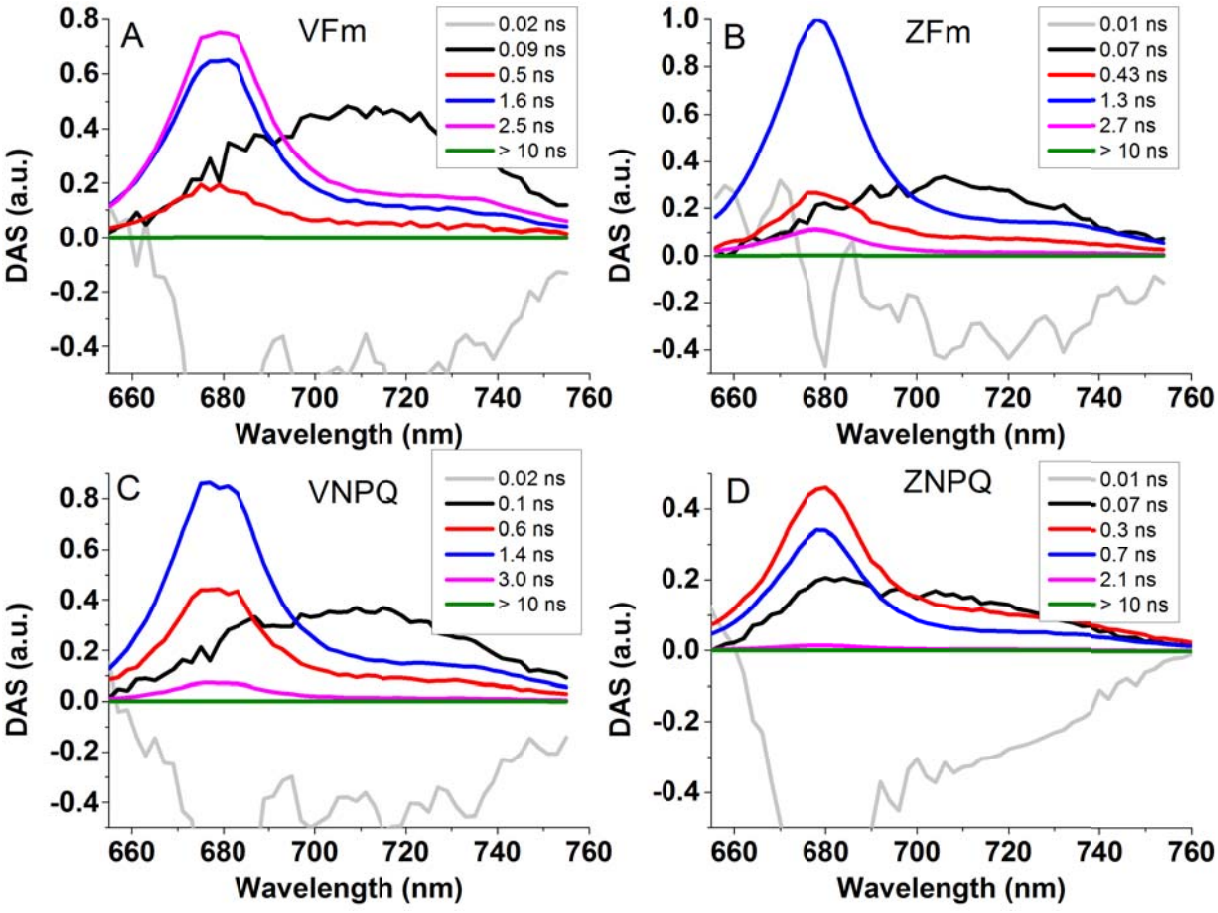

Figure S 10: Global analysis results of the SPC measurements. For the two samples, V and Z as described earlier, two conditions analog to the PAM measurement were probed: closed unquenched ('Fm') and closed quenched ('NPQ'). Shown are the decay associated spectra (DAS) with the estimated lifetimes in the legends. Spectra are normalized to the maximum of the first DAS, except in the case of ZFm where the 4th DAS had the largest amplitude.

Target analysis result

From the global analysis results it is not possible to directly obtain the quantum yield parameters that can be related to the PAM fluorometry data, but it serves as a starting point for a more detailed target analysis which takes into account the different contributions originating from LHCII-PSII and PSI and the different levels of quenching.

To account for the observation of three lifetimes with a similar spectral shape a LHCII-PSII compartment is placed in equilibrium with two (dark) radical pair states, i.e. assuming reversible charge separation, see Figure S 11A. The LHCII-PSII compartment is assumed to be fully equilibrated within the duration of the IRF. The only difference in the model between the four datasets was the quenching rate Q from LHCII-PSII (shown in Figure S 11B) and the shape of the Species Associated Spectra (SAS, c.f. Figure S 11D).). The spectral freedom was needed because the SAS of the LHCII-PSII compartment in the V datasets was less peaked than in the Z datasets irrespective of the Fm or NPQ condition. No evidence was found for an additional quenching site, e.g. in the form of detached LHCII as recently reviewed in [8].

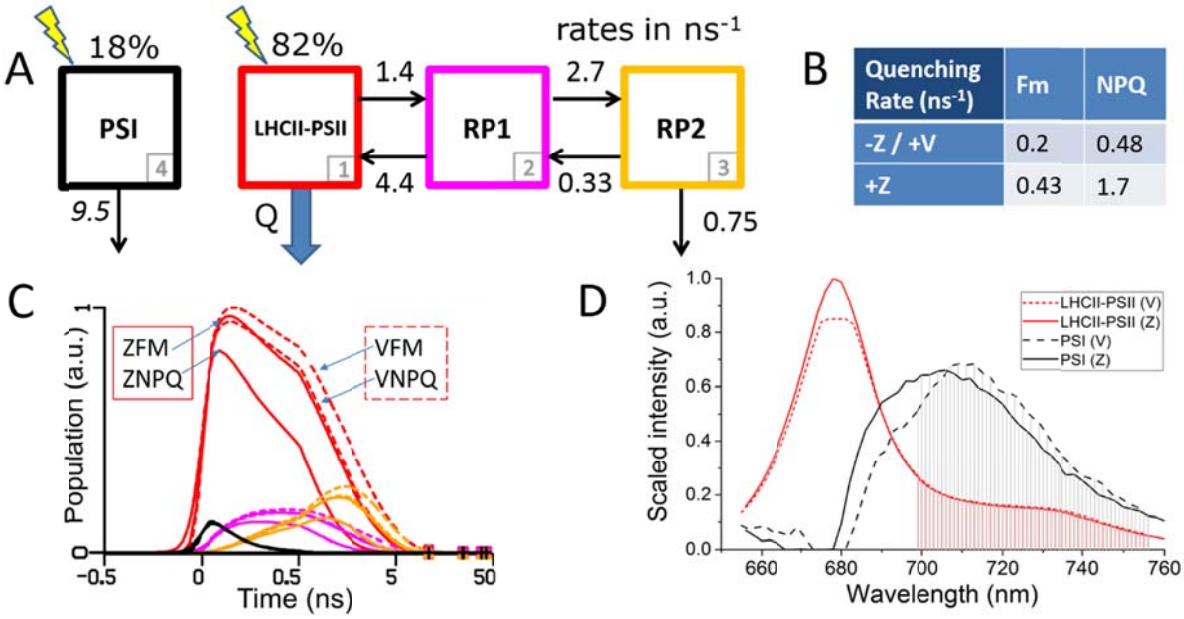

Figure S 11: Overview of simultaneous target analysis results on the four datasets. (A) Target model for time-resolved emission from Chloroplasts at RT excited at 470 nm. All rates (in 1/ns) are fitted parameters with 10% standard error. The input percentages are estimated from an equal SAS area constraint [9]. (B) The quenching rate indicated by Q in the target model for the four different datasets. (C) The population profiles of the different components of the target model. The time axis is linear from -0.5 to 0.5 ns and logarithmic thereafter. (D) The SAS corresponding to the target model for the V datasets (solid) and the Z datasets, with the spectra linked between the Fm and the NPQ state for both. The shading reflects the spectral area used to calculate the relative fluorescence quantum yield as observed by a PAM fluorometer.

Note that whereas in the V samples the quenching rate Q increases from 0.2 in Fm to only 0.48/ns in the NPQ condition, in the ZFm case it is already 0.43/ns. This rate then increases to 1.7/ns in ZNPQ. The quenching is clearly visible in the population profiles in Figure S 11C. Finally the target model can be used to make an estimate for the relative fluorescence quantum yield at the detection wavelengths of the PAM instrument. The steady state concentration levels for each compartment computed from the target analysis are shown in Table S 3.

By multiplying the steady state concentration (which is the integrated area under the population profiles in Figure S 11C) of a fluorescent compartment (i.e. LHCII-PSII, PSI) with the area under its SAS estimated from target analysis (see Figure S 11, panel D), for the relevant integration window of the PAM detector, its relative quantum yield can

be calculated. The calculated quantum yields Φ^{PSII} and Φ^{PSI}, normalized to the yield of PSII in the VFm dataset, can be found in the two rightmost columns of Table S 3.

	LHCII-PSII	RP1	RP2	PSI		φ_{PSII}	φ_{PSI}
VFm	1.402	0.307	0.777	0.019		1.00	0.041
VNPQ	0.913	0.200	0.506	0.019		0.65	0.041
ZFm	0.968	0.212	0.537	0.019		0.68	0.038
ZNPQ	0.379	0.083	0.210	0.019		0.27	0.038

Table S 3: The steady state (integrated) concentrations of the different components in the target analysis depicted in Figure S 11, and the relative quantum yields for PSII and PSI (excited at 470 nm) calculated by multiplying the steady state concentration with the area under its SAS for the region $700 < \lambda < 755\,\text{nm}$.

The relative estimated quantum yield for PSII between the four different cases is largely independent of the excitation wavelength and can therefore be directly compared with what is estimated from PAM fluorometry data regardless of the measuring light used, but the relative yield between PSII and PSI is dependent on the excitation wavelength and cannot always directly be compared. From Table S 3it can be seen that the contribution of PSI according to this target analysis of time-resolved data excited at 470 nm is on the order of a few percent. In the case of the most heavily quenched sample (ZNPQ) the relative contribution is a bit more than 10%. The PAM data reported in this paper was obtained with 620 nm measuring light thus the relative yields are not necessarily comparable. In other work it has been shown that with 624 nm excitation the contribution of PSI to Fo could be as much as 24% in Arabidopsis leaves [10]. This means that the relative quantum yield of PSI for the PAM data (Φ^{PSI}_{PAM}) could be as much as 24% of 0.2, i.e. $\Phi^{PSI} = 0.05$. Assuming a PSI to PSII stoichiometry of 1:1 the effect of including this contribution of PSI has been investigated and the results for the V dataset are reported in Figure S 8 and Figure S 9. The only effect is a small change in the estimated PSII quantum yields: $\Phi^{PSII}_{ou} = 0.16$, $\Phi^{PSII}_{cu} = 0.93$, $\Phi^{PSII}_{oq} = 0.12$, $\Phi^{PSII}_{cq} = 0.37$, $\Phi^{PSI} = 0.05$. Because PSI contributes only an offset (no closing or quenching dynamics) the data could still be fitted equally well.

At this point it makes sense to compare the quantum yields estimated from PAM fluorometry as shown in Figure 9, Figure 10, and Table 1 with those estimated from the target analysis of time-resolved fluorescence as shown in Figure S 11 and summarized in Table S 3. The quantum yields that could be estimated from both techniques are shown in Table S 4.

Dataset	QY label	rel. yield. SPC	rel. yield. PAM
'VFm'	$\Phi^{PSII,V}_{cu}$	1.00	1.00
'VNPQ'	$\Phi^{PSII,V}_{cq}$	0.65	0.41
'ZFm'	$\Phi^{PSII,Z}_{cu}$	0.68	0.67
'ZNPQ'	$\Phi^{PSII,Z}_{cq}$	0.27	0.23

Table S 4: The relative quantum yields for the different states of PSII as could be estimated from SPC data or PAM data.

The quantum yields estimated via either technique are relative to the quantum yield obtained in the Fm case of the V sample. In the case of the PAM fluorometry measurements this is done by normalizing the data to the maximal level of fluorescence in darkness (Fm) where it can be assumed that the only contribution is PSII closed unquenched. In the case of the time-resolved measurement the integrated contribution of LHCII-PSII in the VFm dataset is defined to be 1, the LHCII-PSII contributions in the other datasets are related to this. In the time-resolved data the quantum yield is corrected for the PSI contribution, meaning a small relative error between the two methods is to be expected. Despite this there is considerable consistency in the estimated quantum yields, except perhaps for the VNPQ case.

However it should be noted here that the limited time-resolution of the TCSPC setup (≈110 ps FWHM) meant that it was not possible to reliably quantify quenching processes faster than this, meaning that in the SPC measurement the quantum yield can easily be overestimated due to underestimating the amount of NPQ taking place at early timescales, whereas the yield estimated from the PAM is a reflection of the true quantum yield. This discrepancy could be further investigated by obtaining time-resolved measurements with a much higher time-resolution, for instance using a streak camera setup [11]. Also from the results of the analysis of the PAM curve for the V dataset presented in Figure 9 it can be seen that making sure that the excitation pressure is high enough to keep all RC continuously closed is challenging. The VNPQ case could reflect a mixture of open/closed as well as quenched/unquenched.

Simulations using the Matuszynska et al. 2016 model

Thanks to the availability of the complete simulation source code of the model [12] it was possible to adapt our own light protocol and use it as input for their model. Note that the model was calibrated for the simulation of PAM fluorometry on *Arabidopsis* leafs and not spinach chloroplast, which might explain some inaccuracies in the prediction. Following the same open source philosophy the source code to reproduce these figures is provided in a supplemental file included with this SI. Below follows a brief description in words.

Read in our own raw data (plain csv file) and extract the column with the V fluorescence trace.
Read in our own light protocol stored as two separate files (json format), one containing the timing information on the saturating pulses and the other containing information about the light regimes. Convert this light protocol to the format required by the model.
Initialize the model (type: 'Arabidopsis') with the default parameters and initialize the simulation.
Integrate the model over the times provided by the light protocol.
Extract the PSII state variables (open: B_0; closed B_2) and the degree of quenching Q(t), required for the plotting.
The simulated fluorescence quantum yield Φ can now be described as the sum of the quantum yield in PSII state 0 (open) Φ_{st0} and PSII in state 2 (closed) Φ_{st2}:

$$\begin{aligned}\Phi_{st0}(t) &= k_F / (k_F + k_H * Q(t) + k_{PQ}) * B_0(t)\\ \Phi_{st2}(t) &= k_F / (k_F + k_H * Q(t)) * B_2(t)\\ \Phi(t) &= (\Phi_{st0}(t) + \Phi_{st2}(t)) / \max(\Phi_{st0} + \Phi_{st2})\end{aligned} \qquad \text{Eq.S30}$$

where k_F is the rate of intrinsic fluorescence decay, k_H is the rate of quenching (dissipated as heat) and k_{PQ} is the rate of photochemistry. The rate of NPQ is given by k_H*Q(t), which is modulated by the quencher activity Q which is in turn dependent on the relative concentration of PsbS [PsbS] and Zeaxanthin [Zx], defined as:

$$\begin{aligned}Q = {} & \gamma_0(1-Z_s)[\mathrm{PsbS}] + \gamma_1(1-Z_s)[\mathrm{PsbS}^P]\\ & + \gamma_2 Z_s[\mathrm{PsbS}^P] + \gamma_3 Z_s[\mathrm{PsbS}]\end{aligned} \qquad \text{Eq.S31}$$

where $Z_s = \dfrac{[Zx]}{[Zx] + k_{ZSat}}$ reflects the contribution of Zx to the quenching and k_{ZSat} is a half-saturation constant. The γ parameters were fitted by [12].

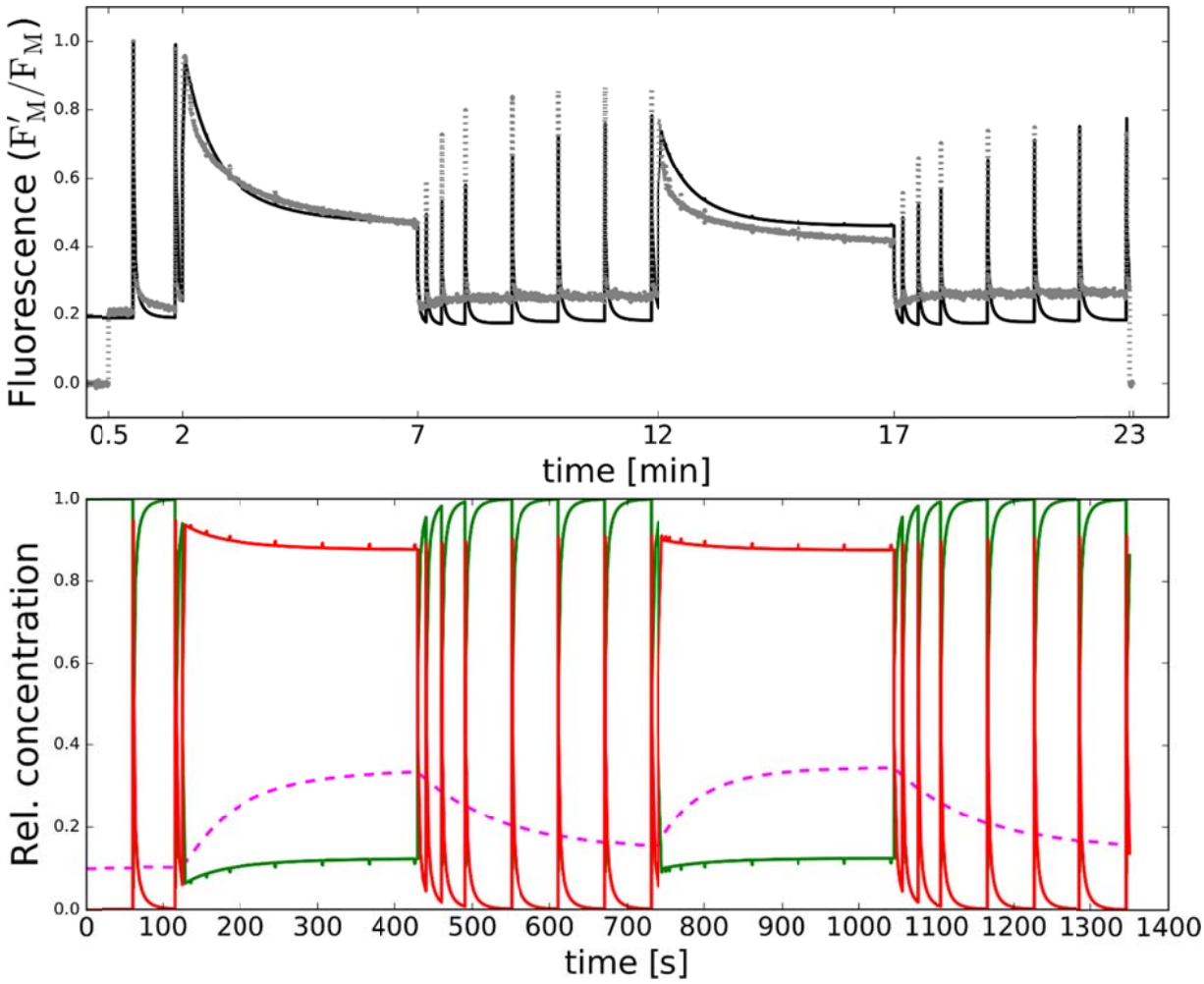

Figure S 12 Predicted fluorescence yield (see Eq.S30) and decomposition using the model published in [12] version 9d46f46 available from https://github.com/QTB-HHU/npqmodel. Top panel shows the predicted fluorescence (solid black) and overlaid the V dataset from Figure 2. Bottom panel shows the decomposition in terms of open PSII (green) and closed PSII (red), in addition the quenching curve Q is shown in magenta.

The clear advantage that an underlying biophysical model provides is that it allows for the investigation of other non-directly observable physical quantities such as the lumenal pH and the relative PsbS and Zeaxanthin concentrations as demonstrated in Figure S 13.

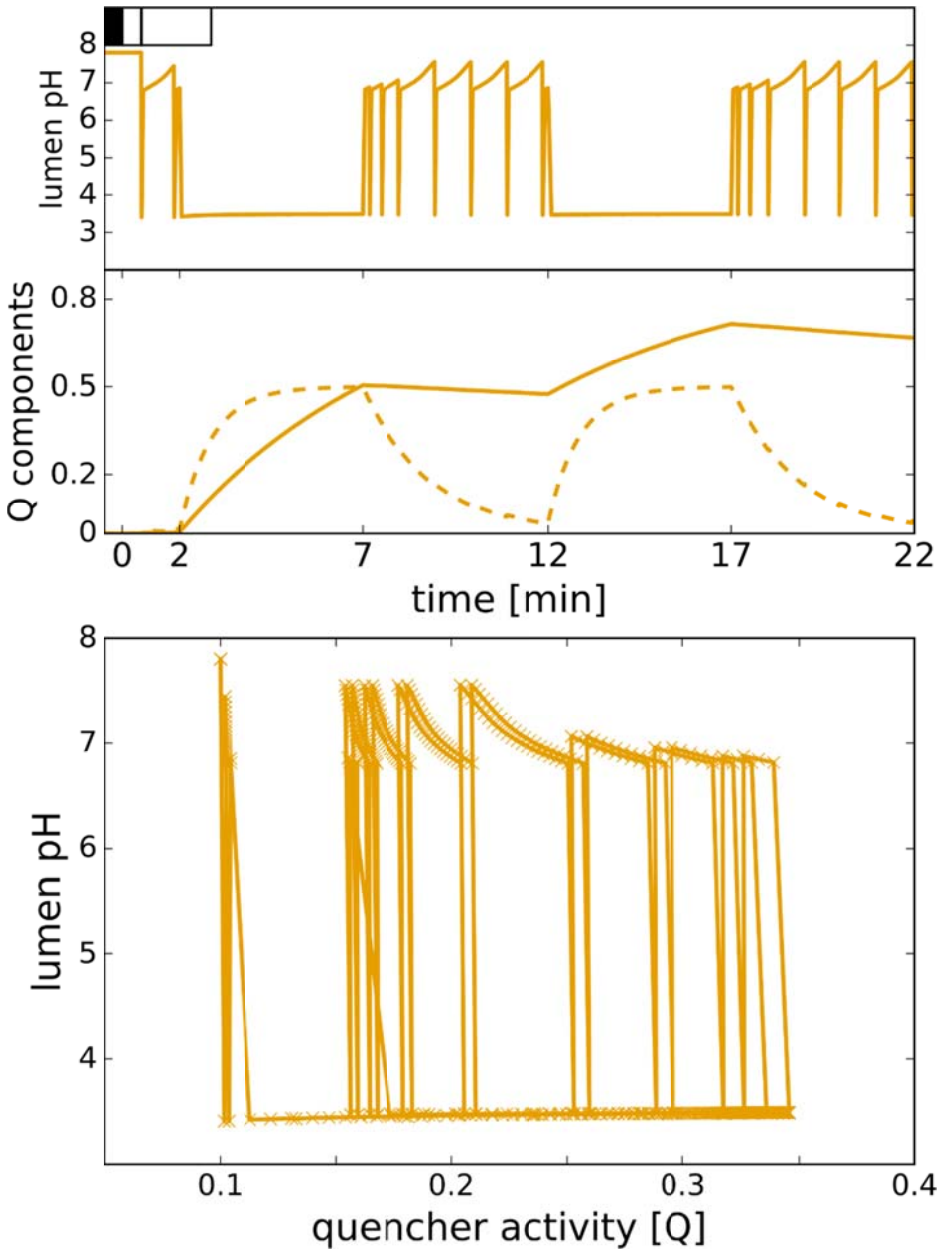

Figure S 13. In analogy to Figure 5 from [12], (top panel) the visualization of lumenal pH changes in the response to our light protocol. (middle panel) the dynamics of the quenching components (solid line for the relative zeaxanthin concentration, dashed line for the ratio of protonated PsbS), (bottom panel) The phase plane trajectories of the quenching variable (Q) and the lumenal pH during our light protocol.

References

[1] A.M. Acuna, J.J. Snellenburg, M. Gwizdala, D. Kirilovsky, R. van Grondelle, I.H.M. van Stokkum, Resolving the contribution of the uncoupled phycobilisomes to cyanobacterial pulse-amplitude modulated (PAM) fluorometry signals, Photosynth Res, 127 (2016) 91-102.
[2] I.H.M. van Stokkum, D.S. Larsen, R. van Grondelle, Global and target analysis of time-resolved spectra, Biochim Biophys Acta, 1657 (2004) 82-104.
[3] E. Belgio, M.P. Johnson, S. Jurić, A.V. Ruban, Higher plant photosystem II light-harvesting antenna, not the reaction center, determines the excited-state lifetime-both the maximum and the nonphotochemically quenched., Biophysical journal, 102 (2012) 2761-2771.
[4] M.P. Johnson, M.L. Pérez-Bueno, A. Zia, P. Horton, A.V. Ruban, The zeaxanthin-independent and zeaxanthin-dependent qE components of nonphotochemical quenching involve common conformational changes within the photosystem II antenna in Arabidopsis., Plant physiology, 149 (2009) 1061-1075.
[5] G.H. Golub, V. Pereyra, The Differentiation of Pseudo-Inverses and Nonlinear Least Squares Problems Whose Variables Separate, SIAM Journal on Numerical Analysis, 10 (1973) 413-432.
[6] K.M. Mullen, I.H.M. van Stokkum, TIMP: An R Package for Modeling Multi-Way Spectroscopic Measurements, Journal of Statistical Software, 18 (2007).
[7] J.J. Snellenburg, S.P. Laptenok, R. Seger, K.M. Mullen, I.H.M.v. Stokkum, Glotaran: A Java-Based Graphical User Interface for the R Package TIMP, Journal of Statistical Software, 49 (2012).
[8] A.R. Holzwarth, P. Jahns, Non-photochemical quenching mechanisms in intact organisms as derived from ultrafast-fluorescence kinetic studies, in: Non-Photochemical Quenching and Energy Dissipation in Plants, Algae and Cyanobacteria, Springer, 2014, pp. 129-156.
[9] J.J. Snellenburg, J.P. Dekker, R. van Grondelle, I.H.M. van Stokkum, Functional compartmental modeling of the photosystems in the thylakoid membrane at 77 K, J Phys Chem B, 117 (2013) 11363-11371.
[10] E.E. Pfündel, C. Klughammer, A. Meister, Z.G. Cerovic, Deriving fluorometer-specific values of relative PSI fluorescence intensity from quenching of F0 fluorescence in leaves of Arabidopsis thaliana and Zea mays, Photosynthesis Research, 114 (2013) 189-206.
[11] I.H.M. van Stokkum, B. van Oort, F. van Mourik, B. Gobets, H. van Amerongen, (Sub)-picosecond spectral evolution of fluorescence studied with a synchroscan streak-camera system and target analysis, in: Biophysical techniques in photosynthesis, Springer, 2008, pp. 223-240.
[12] A. Matuszyńska, S. Heidari, P. Jahns, O. Ebenhöh, A mathematical model of non-photochemical quenching to study short-term light memory in plants, Biochimica et Biophysica Acta (BBA) - Bioenergetics, 1857 (2016) 1860-1869.